

Renormalization constants for 2-twist operators in twisted mass QCD

C. Alexandrou ^{a,b}, M. Constantinou ^a, T. Korzec ^c, H. Panagopoulos ^a, F. Stylianou ^a

^a *Department of Physics, University of Cyprus, PoB 20537, 1678 Nicosia, Cyprus*

^b *Computation-based Science and Technology Research Center,*

The Cyprus Institute, 15 Kypranoros Str., 1645 Nicosia, Cyprus

^c *Institut für Physik, Humboldt Universität zu Berlin, Newtonstrasse 15, 12489 Berlin, Germany **

(Dated: February 14, 2022)

Perturbative and non-perturbative results on the renormalization constants of the fermion field and the twist-2 fermion bilinears are presented with emphasis on the non-perturbative evaluation of the one-derivative twist-2 vector and axial vector operators. Non-perturbative results are obtained using the twisted mass Wilson fermion formulation employing two degenerate dynamical quarks and the tree-level Symanzik improved gluon action. The simulations have been performed for pion masses in the range of about 450-260 MeV and at three values of the lattice spacing a corresponding to $\beta = 3.9, 4.05, 4.20$. Subtraction of $\mathcal{O}(a^2)$ terms is carried out by performing the perturbative evaluation of these operators at 1-loop and up to $\mathcal{O}(a^2)$. The renormalization conditions are defined in the RI'-MOM scheme, for both perturbative and non-perturbative results. The renormalization factors, obtained for different values of the renormalization scale, are evolved perturbatively to a reference scale set by the inverse of the lattice spacing. In addition, they are translated to $\overline{\text{MS}}$ at 2 GeV using 3-loop perturbative results for the conversion factors.

PACS numbers: 11.15.Ha, 12.38.Gc, 12.38.Aw, 12.38.-t, 14.70.Dj

Keywords: Lattice QCD, Twisted mass fermions, Renormalization constants

*Electronic address: alexand@ucy.ac.cy, marthac@ucy.ac.cy, korzec@physik.hu-berlin.de, haris@ucy.ac.cy, fstyl01@ucy.ac.cy

I. INTRODUCTION

Simulations in lattice QCD have advanced remarkably in the past couple of years reaching within 100 MeV of the physical pion mass. This progress is due to theoretical improvements in defining the theory on the lattice and to algorithmic improvements that give a better scaling behavior as the quark mass decreases. These developments, combined with the tremendous increase in computational power, have made *ab initio* calculations of key observables on hadron structure in the chiral regime feasible enabling comparison with experiment. The hadron mass spectrum [1, 2] illustrates the good quality of lattice results that can be obtained. The agreement with experiment is a validation of the lattice approach, and justifies the computation of hadron observables beyond hadron masses, such as form factors and parton distribution functions. Both form factors and parton distribution functions can be obtained from the so-called generalized parton distributions (GPDs) in certain limiting cases. GPDs provide detailed information on the internal structure of hadron in terms of both the longitudinal momentum fraction and the total momentum transfer squared. Beyond the information that the form factors yield, such as size, magnetization and shape, GPDs encode additional information, relevant for experimental investigations, such as the decomposition of the total hadron spin into angular momentum and spin carried by quarks and gluons.

GPDs are single particle matrix elements of the light-cone operator [3, 4],

$$\mathcal{O}_\Gamma^f(x) = \int \frac{d\lambda}{4\pi} e^{i\lambda x} \bar{\psi}^f(-\frac{\lambda}{2}n) \Gamma \cdot n \mathcal{P} e^{ig \int_{-\lambda/2}^{\lambda/2} d\alpha n \cdot A(\alpha n)} \psi^f(\frac{\lambda}{2}n), \quad (1)$$

where n is a light-cone vector, and \mathcal{P} denotes a path-ordering of the gauge fields in the exponential. Such matrix elements cannot be calculated directly in lattice QCD. However, $\mathcal{O}(x)$ can be expanded in terms of local twist-two operators

$$\mathcal{O}_\Gamma^{f, \{\mu_1 \mu_2 \dots \mu_n\}} = \bar{\psi}^f \Gamma^{\{\mu_1} i \overleftrightarrow{D}^{\mu_2} \dots i \overleftrightarrow{D}^{\mu_n\}} \psi^f \quad (2)$$

where $\overleftrightarrow{D} = \frac{1}{2}(\overrightarrow{D} - \overleftarrow{D})$ and $\{\mu_1, \dots, \mu_n\}$ denotes symmetrization of indices and subtraction of traces. In this work we focus on the Dirac structures $\Gamma = \gamma^\mu, \gamma_5 \gamma^\mu$ and $\gamma^5 \sigma^{\mu\nu}$ ($\sigma^{\mu\nu} = [\gamma^\mu, \gamma^\nu]/2$), which are referred to as vector $\mathcal{O}_V^f(x)$, axial-vector $\mathcal{O}_A^f(x)$ and tensor $\mathcal{O}_T^f(x)$ operators, respectively. In lattice QCD we consider matrix elements of such bilinear operators. A number of lattice groups are producing results on nucleon form factors and first moments of structure functions closer to the physical regime both in terms of pion mass as well as in terms of the continuum limit [5–11]. While experiments are able to measure convolutions of GPDs, lattice QCD allows us to extract hadron matrix elements for the twist-2 operators, which can be expressed in terms of generalized form factors.

In order to compare hadron matrix elements of these local operators to experiment one needs to renormalize them. The aim of this paper is to calculate non-perturbatively the renormalization factors of the above twist-two fermion operators within the twisted mass formulation. We show that, although the lattice spacings considered in this work are smaller than 1 fm, $\mathcal{O}(a^2)$ terms are non-negligible and significantly larger than statistical errors. We therefore compute the $\mathcal{O}(a^2)$ -terms perturbatively and subtract them from the non-perturbative results. This subtraction suppresses lattice artifacts considerably depending on the operator under study and leads to a more accurate determination of the renormalization constants. Preliminary results of this work have been published in Refs. [11, 12].

The paper is organized as follows: in Section II we give the expressions for the fermion and gluon actions we employed, and define the twist-two operators. Section III concentrates on the perturbative procedure, and the $\mathcal{O}(a^2)$ -corrected expressions for the renormalization constants Z_q and $Z_\mathcal{O}$. Section IV focuses on the non-perturbative computation, where we explain the different steps of the calculation. Moreover, we provide the renormalization prescription of the RI'-MOM scheme, and we discuss alternative ways for its application. The main results of this work are presented in Section V: the reader can find numerical values for the Z-factors of the twist-2 operators, which are computed non-perturbatively and corrected using the perturbative $\mathcal{O}(a^2)$ terms presented in Section III. Since in general Z-factors depend on the renormalization scale, we also provide results in the RI'-MOM scheme at a reference scale, $\mu \sim 1/a$. For comparison with phenomenological and experimental results, we convert the Z-factors to the $\overline{\text{MS}}$ scheme at 2 GeV. In Section VI we give our conclusions.

A forthcoming paper [13] will focus on the perturbative procedure and will present results for local fermion operators (scalar, pseudoscalar, vector, axial, tensor).

II. FORMULATION

A. Lattice action

For the gauge fields we use the tree-level Symanzik improved gauge action [14], which includes besides the plaquette term $U_{x,\mu,\nu}^{1 \times 1}$ also rectangular (1×2) Wilson loops $U_{x,\mu,\nu}^{1 \times 2}$

$$S_g = \frac{\beta}{3} \sum_x \left(b_0 \sum_{\substack{\mu, \nu=1 \\ 1 \leq \mu < \nu}}^4 \{1 - \text{Re Tr}(U_{x,\mu,\nu}^{1 \times 1})\} + b_1 \sum_{\substack{\mu, \nu=1 \\ \mu \neq \nu}}^4 \{1 - \text{Re Tr}(U_{x,\mu,\nu}^{1 \times 2})\} \right) \quad (3)$$

with $\beta = 2 N_c / g_0^2$, $b_1 = -1/12$ and the (proper) normalization condition $b_0 = 1 - 8b_1$. Note that at $b_1 = 0$ this action becomes the usual Wilson plaquette gauge action.

The fermionic action for two degenerate flavors of quarks in twisted mass QCD is given by

$$S_F = a^4 \sum_x \bar{\chi}(x) (D_W[U] + m_0 + i\mu_0 \gamma_5 \tau^3) \chi(x) \quad (4)$$

with τ^3 the Pauli matrix acting in the isospin space, μ_0 the bare twisted mass and D_W the massless Wilson-Dirac operator defined as

$$D_W[U] = \frac{1}{2} \gamma_\mu (\vec{\nabla}_\mu + \vec{\nabla}_\mu^*) - \frac{ar}{2} \vec{\nabla}_\mu \vec{\nabla}_\mu^* \quad (5)$$

where

$$\vec{\nabla}_\mu \psi(x) = \frac{1}{a} \left[U_\mu(x) \psi(x + a\hat{\mu}) - \psi(x) \right] \quad \text{and} \quad \vec{\nabla}_\mu^* \psi(x) = -\frac{1}{a} \left[U_\mu^\dagger(x - a\hat{\mu}) \psi(x - a\hat{\mu}) - \psi(x) \right] \quad (6)$$

For completeness we also provide the definition of the backward derivatives

$$\overleftarrow{\nabla}_\mu \bar{\psi}(x) = \frac{1}{a} \left[\bar{\psi}(x + a\hat{\mu}) U_\mu^\dagger(x) - \bar{\psi}(x) \right] \quad \text{and} \quad \overleftarrow{\nabla}_\mu^* \bar{\psi}(x) = -\frac{1}{a} \left[\bar{\psi}(x - a\hat{\mu}) U_\mu(x - a\hat{\mu}) - \bar{\psi}(x) \right] \quad (7)$$

Maximally twisted Wilson quarks are obtained by setting the untwisted bare quark mass m_0 to its critical value m_{cr} , while the twisted quark mass parameter μ_0 is kept non-vanishing in order to give the light quarks their mass. In Eq. (4) the quark fields χ are in the so-called “twisted basis”. The “physical basis” is obtained for maximal twist by the simple transformation

$$\psi(x) = \exp\left(\frac{i\pi}{4} \gamma_5 \tau^3\right) \chi(x), \quad \bar{\psi}(x) = \bar{\chi}(x) \exp\left(\frac{i\pi}{4} \gamma_5 \tau^3\right) \quad (8)$$

In terms of the physical fields the action is given by

$$S_F^\psi = a^4 \sum_x \bar{\psi}(x) \left(\frac{1}{2} \gamma_\mu [\vec{\nabla}_\mu + \vec{\nabla}_\mu^*] - i\gamma_5 \tau^3 \left(-\frac{ar}{2} \vec{\nabla}_\mu \vec{\nabla}_\mu^* + m_{\text{cr}} \right) + \mu_0 \right) \psi(x) \quad (9)$$

In this work we consider twist-two operators with one derivative, which are given in the twisted basis as follows

$$\mathcal{O}_{\text{DV}}^{\{\mu\nu\}} = \bar{\chi} \gamma_{\{\mu} \overleftrightarrow{D}_{\nu\}} \tau^a \chi = \begin{cases} \bar{\psi} \gamma_5 \gamma_{\{\mu} \overleftrightarrow{D}_{\nu\}} \tau^2 \psi & a = 1 \\ -\bar{\psi} \gamma_5 \gamma_{\{\mu} \overleftrightarrow{D}_{\nu\}} \tau^1 \psi & a = 2 \\ \bar{\psi} \gamma_{\{\mu} \overleftrightarrow{D}_{\nu\}} \tau^3 \psi & a = 3 \end{cases} \quad (10)$$

$$\mathcal{O}_{\text{DA}}^{\{\mu\nu\}} = \bar{\chi} \gamma_5 \gamma_{\{\mu} \overleftrightarrow{D}_{\nu\}} \tau^a \chi = \begin{cases} \bar{\psi} \gamma_{\{\mu} \overleftrightarrow{D}_{\nu\}} \tau^2 \psi & a = 1 \\ -\bar{\psi} \gamma_{\{\mu} \overleftrightarrow{D}_{\nu\}} \tau^1 \psi & a = 2 \\ \bar{\psi} \gamma_5 \gamma_{\{\mu} \overleftrightarrow{D}_{\nu\}} \tau^3 \psi & a = 3 \end{cases} \quad (11)$$

$$\mathcal{O}_{\text{DT}}^{\mu\{\nu\rho\}} = \bar{\chi} \gamma_5 \sigma_{\mu\{\nu} \overleftrightarrow{D}_{\rho\}} \tau^a \chi = \begin{cases} \bar{\psi} \gamma_5 \sigma_{\mu\{\nu} \overleftrightarrow{D}_{\rho\}} \tau^a \psi & a = 1, 2 \\ -i \bar{\psi} \sigma_{\mu\{\nu} \overleftrightarrow{D}_{\rho\}} \mathbb{1} \psi & a = 3 \end{cases} \quad (12)$$

with the covariant derivative defined as

$$\overleftrightarrow{D} = \frac{1}{2} \left[\frac{(\vec{\nabla}_\mu + \vec{\nabla}_\mu^*)}{2} - \frac{(\overleftarrow{\nabla}_\mu + \overleftarrow{\nabla}_\mu^*)}{2} \right]. \quad (13)$$

The above operators are symmetrized over two Lorentz indices and are made traceless

$$\mathcal{O}^{\{\sigma\tau\}} \equiv \frac{1}{2} (\mathcal{O}^{\sigma\tau} + \mathcal{O}^{\tau\sigma}) - \frac{1}{4} \delta^{\sigma\tau} \sum_\lambda \mathcal{O}^{\lambda\lambda}. \quad (14)$$

This definition avoids mixing with lower dimension operators. We denote the corresponding Z-factors by Z_{DV}^a , Z_{DA}^a , Z_{DT}^a . In a massless renormalization scheme the renormalization constants are defined in the chiral limit, where isospin symmetry is exact. Hence, the same value for Z is obtained independently of the value of the isospin index a and therefore we drop the a index on the Z -factors from here on. However, one must note that, for instance, the physical $\bar{\psi} \gamma_{\{\mu} \overleftrightarrow{D}_{\nu\}} \tau^1 \psi$ is renormalized with Z_{DA} , while $\bar{\psi} \gamma_{\{\mu} \overleftrightarrow{D}_{\nu\}} \tau^3 \psi$ requires the Z_{DV} , which differ from each other even in the chiral limit.

The one derivative operators fall into different irreducible representations of the hypercubic group, depending on the choice of indices. Hence, we distinguish between

$$\mathcal{O}_{\text{DV1}} = \mathcal{O}_{\text{DV}} \text{ with } \mu = \nu \quad (15)$$

$$\mathcal{O}_{\text{DV2}} = \mathcal{O}_{\text{DV}} \text{ with } \mu \neq \nu \quad (16)$$

$$\mathcal{O}_{\text{DA1}} = \mathcal{O}_{\text{DA}} \text{ with } \mu = \nu \quad (17)$$

$$\mathcal{O}_{\text{DA2}} = \mathcal{O}_{\text{DA}} \text{ with } \mu \neq \nu \quad (18)$$

$$\mathcal{O}_{\text{DT1}} = \mathcal{O}_{\text{DT}} \text{ with } \mu \neq \nu = \rho \quad (19)$$

$$\mathcal{O}_{\text{DT2}} = \mathcal{O}_{\text{DT}} \text{ with } \mu \neq \nu \neq \rho \neq \mu \quad (20)$$

Thus, Z_{DV1} will be different from Z_{DV2} , but renormalized matrix elements of the two corresponding operators will be components of the same tensor in the continuum limit. \mathcal{O}_{DT1} is sufficient to extract all generalized form factors of the one derivative tensor operators. Although, in this work, we will calculate non-perturbatively only the renormalization constants for the vector and axial-vector operator, we will provide the perturbative $\mathcal{O}(a^2)$ terms also for the tensor operators.

III. PERTURBATIVE PROCEDURE

Here we present our results for the renormalization factor of the fermion field, Z_q , that enters the evaluation of the twist-2 operators, and we also calculate Z_{DV} , Z_{DA} , Z_{DT} . Our calculation is performed in 1-loop perturbation theory to $\mathcal{O}(a^2)$. Extending the calculation up to $\mathcal{O}(a^2)$ brings in new difficulties, compared to lower order in a ; for instance, there appear new types of singularities. The procedure to address this issue is extensively described in Ref. [15]. Many IR singularities encountered at $\mathcal{O}(a^2)$ would persist even up to 6 dimensions, making their extraction more delicate. In addition to that, there appear Lorentz non-invariant contributions in $\mathcal{O}(a^2)$ terms, such as $\sum_\mu p_\mu^4/p^2$, where p is the external momentum; as a consequence, the Z-factors also depend on such terms. The knowledge of the order a^2 terms is a big advantage for non-perturbative estimates, since they can eliminate possible large lattice artifacts, once the $\mathcal{O}(a^2)$ perturbative terms are subtracted.

For all our perturbative results we employ a general fermion action, which includes the clover parameter, c_{SW} , and non-zero Lagrangian mass, m . For the fermion field renormalization we also have a finite twisted mass parameter, μ_0 , so we can explore its μ_0 dependence. Only the renormalization factors of the twist-2 operators are obtained at $\mu_0 = 0$, but we still consider $m \neq 0$. For gluons we use Symanzik improved actions (Plaquette, Tree-level Symanzik, Iwasaki, TILW, DBW2) [15]. The purpose of using such general fermion and gluon actions is to make our results applicable to a variety of actions used nowadays in simulations. The expressions for the matrix elements and the Z-factors are given in a general covariant gauge, and their dependence on the coupling constant, the external momentum, the masses and the clover parameter is shown explicitly.

A. Fermion field renormalization

The fermion action used for the inverse fermion propagator improvement is a combination of Wilson/clover/twisted mass fermions, given by

$$S_F = \sum_{x,\nu} \bar{\psi}(x) \left[\frac{\gamma_\nu}{2} (\vec{\nabla}_\nu + \vec{\nabla}_\nu^*) - \frac{ar}{2} \vec{\nabla}_\nu^* \vec{\nabla}_\nu + m_0 + i\mu_0 \gamma_5 \tau^3 - \sum_\rho \frac{1}{4} c_{SW} \sigma_{\rho\nu} \hat{F}_{\rho\nu}(x) \right] \Psi(x) \quad (21)$$

All quantities appearing in Eq. (21) are defined in Ref. [15]. There are two 1-loop diagrams involved in this particular computation, which are illustrated in Fig. 1.

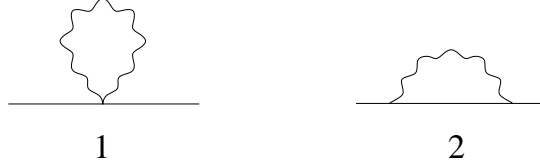


FIG. 1: One-loop diagrams contributing to the fermion propagator. Wavy lines represent gluons and solid lines fermions.

We compute Z_q in the RI'-MOM renormalization scheme, defined as

$$Z_q = \frac{1}{4} \text{Tr} \left[S_{\text{tree}}^{(0)}(p) S^{-1}(p) \right] \Big|_{p_\rho = \mu_\rho} = -\frac{i}{4} \text{Tr} \left[\frac{\frac{1}{a} \sum_\rho \gamma_\rho \sin(a p_\rho)}{\frac{1}{a^2} \sum_\rho \sin^2(a p_\rho)} \cdot S^{-1}(p) \right] \Big|_{p_\rho = \mu_\rho}. \quad (22)$$

For comparison reasons, an additional renormalization prescription was also applied (see Eqs. (56) - (57)). Since we want to take into account all $\mathcal{O}(a^2)$ terms, we perform a Taylor expansion leading to

$$\begin{aligned} Z_q &= -\frac{i}{4} \text{Tr} \left[\frac{\sum_\rho \gamma_\rho (p_\rho - \frac{a^2}{6} p_\rho^3)}{\sum_\rho p_\rho^2} \left(1 + \frac{a^2}{3} \frac{\sum_\rho p_\rho^4}{\sum_\rho p_\rho^2} \right) \cdot S_{1\text{-loop}}^{-1}(p) \right] \Big|_{p_\rho = \mu_\rho} + \mathcal{O}(a^4 g^2, g^4) \\ &= -\frac{i}{4} \text{Tr} \left[\frac{\not{p}}{p^2} \cdot S_{1\text{-loop}}^{-1}(p) - \frac{a^2}{3} \left(\frac{1}{2} \frac{\not{p}^3}{p^2} - \frac{\not{p} p^4}{(p^2)^2} \right) \cdot S_{1\text{-loop}}^{-1}(p) \right] \Big|_{p_\rho = \mu_\rho} + \mathcal{O}(a^4 g^2, g^4). \end{aligned} \quad (23)$$

The trace is taken only over spin indices and $S_{1\text{-loop}}^{-1}$ is the inverse fermion propagator that we computed up to 1-loop and up to $\mathcal{O}(a^2)$. We make the following definitions for convenience: $p^2 \equiv \sum_\rho p_\rho^2$, $p^4 \equiv \sum_\rho p_\rho^4$, $\not{p} = \sum_\rho \gamma_\rho p_\rho$ and $\not{p}^3 \equiv \sum_\rho \gamma_\rho p_\rho^3$. A very important observation is that the $\mathcal{O}(a^2)$ terms depend not only on the magnitude, $\sum_\rho p_\rho^2$, but also on the direction of the external momentum, p_ρ , as manifested by the presence of the terms $\sum_\rho p_\rho^4$. As a consequence, alternative renormalization prescriptions, involving different directions of the renormalization scale $\mu_\rho = p_\rho$, treat lattice artifacts diversely.

For the special choices: $c_{SW} = 0$, $r = 1$ (Wilson parameter), $\lambda = 0$ (Landau gauge), $m_0 = 0$, $\mu_0 = 0$, and for tree-level Symanzik gluons, Z_q can be read from the following trace

$$\begin{aligned} \frac{1}{4} \text{Tr} \left[S_{\text{tree}}^{(0)}(p) S_{1\text{-loop}}^{-1}(p) \right] \Big|_{p_\rho = \mu_\rho} &= 1 + \tilde{g}^2 \left\{ -13.02327272(7) \right. \\ &\quad + a^2 \left[\mu^2 (1.14716212(5) - \frac{73}{360} \ln(a^2 \mu^2)) \right. \\ &\quad \left. \left. + \frac{\sum_\rho \mu_\rho^4}{\mu^2} (2.1064995(2) - \frac{157}{180} \ln(a^2 \mu^2)) \right] \right\} + \mathcal{O}(a^4 g^2, g^4) \end{aligned} \quad (24)$$

where $\tilde{g}^2 \equiv g^2 C_F / (16\pi^2)$, $C_F = (N_c^2 - 1)/(2N_c)$ and $\mu^2 \equiv \sum_\rho \mu_\rho^2$. In Ref. [13] we provide Z_q for $c_{SW} = 0$, $\lambda = 0$ and the dependence on m_0 , μ_0 shown explicitly. Its most general expression (including c_{SW} and λ , as well as a wider choice of values for the parameters entering the Symanzik action) is far too lengthy to be included in paper form (Z_q , Z_{DV} , Z_{DA} , Z_{DT} around: 250, 800, 800, 950 terms respectively); it is provided in electronic form along with Ref. [13].

B. Renormalization of twist-2 operators

Here we present the computation of the amputated Green's functions for the following three twist-2 operators

$$\mathcal{O}_{\text{DV}}^{\{\mu\nu\}} = \frac{1}{2} \left[\bar{\Psi} \gamma_\mu \overleftrightarrow{D}_\nu \Psi + \bar{\Psi} \gamma_\nu \overleftrightarrow{D}_\mu \Psi \right] - \frac{1}{4} \delta_{\mu\nu} \sum_\tau \bar{\Psi} \gamma_\tau \overleftrightarrow{D}_\tau \Psi \quad (25)$$

$$\mathcal{O}_{\text{DA}}^{\{\mu\nu\}} = \frac{1}{2} \left[\bar{\Psi} \gamma_5 \gamma_\mu \overleftrightarrow{D}_\nu \Psi + \bar{\Psi} \gamma_5 \gamma_\nu \overleftrightarrow{D}_\mu \Psi \right] - \frac{1}{4} \delta_{\mu\nu} \sum_\tau \bar{\Psi} \gamma_5 \gamma_\tau \overleftrightarrow{D}_\tau \Psi \quad (26)$$

$$\mathcal{O}_{\text{DT}}^{\mu\{\nu\rho\}} = \frac{1}{2} \left[\bar{\Psi} \gamma_5 \sigma_{\mu\nu} \overleftrightarrow{D}_\rho \Psi + \bar{\Psi} \gamma_5 \sigma_{\mu\rho} \overleftrightarrow{D}_\nu \Psi \right] - \frac{1}{4} \delta_{\nu\rho} \sum_\tau \bar{\Psi} \gamma_5 \sigma_{\mu\tau} \overleftrightarrow{D}_\tau \Psi \quad (27)$$

which, being symmetrized and traceless, have no mixing with lower dimension operators.

The Feynman diagrams that enter our calculation are given below, where the insertion of the twist-2 operator is represented by a cross. We have computed, to $\mathcal{O}(a^2)$, the forward matrix elements of these operators for general

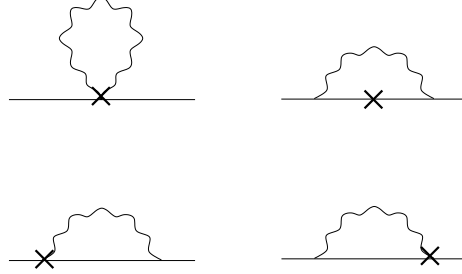


FIG. 2: One-loop diagrams contributing to the computation of the twist-2 operators. A wavy (solid) line represents gluons (fermions). A cross denotes an insertion of the operator under study.

external indices μ, ν (and ρ for the tensor operator), external momentum p , m_0 , g , N_c , a , c_{SW} and λ . Setting $\lambda = 1$ corresponds to the Feynman gauge, whereas $\lambda = 0$ corresponds to the Landau gauge. Our final results were obtained for the 10 sets of Symanzik coefficients we have used in the calculation of Z_q [15].

In order to define $Z_{\mathcal{O}}$, we have used a renormalization prescription which is most amenable to non-perturbative treatment:

$$Z_q^{-1} Z_{\mathcal{O}} \text{Tr} \left[L^{\mathcal{O}}(p) \cdot L_{\text{tree}}^{\mathcal{O}}(p) \right]_{p_\lambda = \mu_\lambda} = \text{Tr} \left[L_{\text{tree}}^{\mathcal{O}}(p) \cdot L_{\text{tree}}^{\mathcal{O}}(p) \right]_{p_\lambda = \mu_\lambda} \quad (28)$$

where $L^{\mathcal{O}}$ denotes the amputated 2-point Green's function of the operators in Eqs. (25) - (27), up to 1-loop and up to $\mathcal{O}(a^2)$. The tree-level expressions of the operators including the $\mathcal{O}(a^2)$ terms are

$$L_{\text{tree}}^{\text{DV1}}(p) = i\gamma_\mu \left(p_\mu - a^2 \frac{p_\mu^3}{6} \right) - \frac{i}{4} \sum_\tau \gamma_\tau \left(p_\tau - a^2 \frac{p_\tau^3}{6} \right) + \mathcal{O}(a^4), \quad L_{\text{tree}}^{\text{DA1}}(p) = \gamma_5 L_{\text{tree}}^{\text{DV1}}(p) \quad (29)$$

$$L_{\text{tree}}^{\text{DV2}}(p) = \frac{i}{2} \left(\gamma_\mu \left(p_\nu - a^2 \frac{p_\nu^3}{6} \right) + \gamma_\nu \left(p_\mu - a^2 \frac{p_\mu^3}{6} \right) \right) + \mathcal{O}(a^4), \quad L_{\text{tree}}^{\text{DA2}}(p) = \gamma_5 L_{\text{tree}}^{\text{DV2}}(p) \quad (30)$$

$$L_{\text{tree}}^{\text{DT1}}(p) = i\gamma_5 \sigma_{\mu\nu} \left(p_\nu - a^2 \frac{p_\nu^3}{6} \right) - \frac{i}{4} \sum_\tau \gamma_5 \sigma_{\mu\tau} \left(p_\tau - a^2 \frac{p_\tau^3}{6} \right) + \mathcal{O}(a^4) \quad (31)$$

$$L_{\text{tree}}^{\text{DT2}}(p) = \frac{i}{2} \gamma_5 \left(\sigma_{\mu\nu} \left(p_\rho - a^2 \frac{p_\rho^3}{6} \right) + \sigma_{\mu\rho} \left(p_\nu - a^2 \frac{p_\nu^3}{6} \right) \right) + \mathcal{O}(a^4) \quad (32)$$

We perform a Taylor expansion up to $\mathcal{O}(a^2)$ in the right hand side of the renormalization condition and it leads to

the following

$$\text{Tr}\left[L_{\text{tree}}^{\text{DV1}}(p) \cdot L_{\text{tree}}^{\text{DV1}}(p)\right] = -2p_\mu^2 - \frac{1}{4}p^2 + \textcolor{red}{a}^2\left(\frac{1}{12}p^4 + \frac{2}{3}p_\mu^4\right) + \mathcal{O}(a^4) = -\text{Tr}\left[L_{\text{tree}}^{\text{DA1}}(p) \cdot L_{\text{tree}}^{\text{DA1}}(p)\right] \quad (33)$$

$$\text{Tr}\left[L_{\text{tree}}^{\text{DV2}}(p) \cdot L_{\text{tree}}^{\text{DV2}}(p)\right] = -p_\mu^2 - p_\nu^2 + \frac{\textcolor{red}{a}^2}{3}(p_\mu^4 + p_\nu^4) + \mathcal{O}(a^4) = -\text{Tr}\left[L_{\text{tree}}^{\text{DA2}}(p) \cdot L_{\text{tree}}^{\text{DA2}}(p)\right] \quad (34)$$

$$\text{Tr}\left[L_{\text{tree}}^{\text{DT1}}(p) \cdot L_{\text{tree}}^{\text{DT1}}(p)\right] = \frac{p^2}{4} + 2p_\nu^2 - \frac{p_\mu^2}{4} - \textcolor{red}{a}^2\left(\frac{p^4}{12} + \frac{2p_\nu^4}{3} - \frac{p_\mu^4}{12}\right) + \mathcal{O}(a^4) \quad (35)$$

$$\text{Tr}\left[L_{\text{tree}}^{\text{DT2}}(p) \cdot L_{\text{tree}}^{\text{DT2}}(p)\right] = p_\nu^2 + p_\rho^2 - \frac{\textcolor{red}{a}^2}{3}(p_\nu^4 + p_\rho^4) + \mathcal{O}(a^4) \quad (36)$$

For the special choices: $m_0 = 0$, $c_{SW} = 0$, $r = 1$, $\lambda = 0$ (Landau gauge), and for tree-level Symanzik gluons, we obtain for the left hand side of Eq. (28)

$$\begin{aligned} \text{Tr}\left[L^{\text{DV1}}(p) \cdot L_{\text{tree}}^{\text{DV1}}(p)\right] &= -2p_\mu^2 - \frac{1}{4}p^2 + \textcolor{red}{a}^2\left(\frac{1}{12}p^4 + \frac{2}{3}p_\mu^4\right) \\ &+ \tilde{g}^2\left\{\frac{4}{3}\frac{p_\mu^4}{p^2} + p^2\left(3.610062(3) - \frac{2}{3}\ln(\textcolor{red}{a}^2 p^2)\right) + p_\mu^2\left(27.54716(3) - \frac{16}{3}\ln(\textcolor{red}{a}^2 p^2)\right) \right. \\ &\quad + \textcolor{red}{a}^2\left[(p^2)^2\left(0.11838(2) + \frac{7}{288}\ln(\textcolor{red}{a}^2 p^2)\right) + p^2 p_\mu^2\left(-0.6573(1) - \frac{299}{180}\ln(\textcolor{red}{a}^2 p^2)\right) \right. \\ &\quad \left. + p^4\left(-1.71886(3) + \frac{397}{720}\ln(\textcolor{red}{a}^2 p^2) - \frac{43}{360}\frac{p_\mu^2}{p^2}\right) \right. \\ &\quad \left. \left. + p_\mu^4\left(-16.1049(5) + \frac{94}{15}\ln(\textcolor{red}{a}^2 p^2) + \frac{29}{90}\frac{p^4}{(p^2)^2} + \frac{169}{45}\frac{p_\mu^2}{p^2}\right)\right]\right\} \\ &+ \mathcal{O}(a^4, g^4) \end{aligned} \quad (37)$$

$$\begin{aligned} \text{Tr}\left[L^{\text{DV2}}(p) \cdot L_{\text{tree}}^{\text{DV2}}(p)\right] &= -p_\mu^2 - p_\nu^2 + \frac{\textcolor{red}{a}^2}{3}(p_\mu^4 + p_\nu^4) \\ &+ \tilde{g}^2\left\{\frac{4}{3}\frac{p_\mu^2 p_\nu^2}{p^2} + (p_\mu^2 + p_\nu^2)\left(15.04575(1) - \frac{8}{3}\ln(\textcolor{red}{a}^2 p^2)\right) \right. \\ &\quad + \textcolor{red}{a}^2\left[(p_\mu^4 + p_\nu^4)\left(-7.1429(1) + \frac{491}{360}\ln(\textcolor{red}{a}^2 p^2)\right) \right. \\ &\quad \left. + (p_\mu^2 + p_\nu^2)\left(p^2\left(-0.13212(3) - \frac{103}{360}\ln(\textcolor{red}{a}^2 p^2)\right) + \frac{353}{720}\frac{p^4}{p^2}\right) \right. \\ &\quad \left. \left. + p_\mu^2 p_\nu^2\left(-4.0096(1) + \frac{1013}{180}\ln(\textcolor{red}{a}^2 p^2) + \frac{29}{90}\frac{p^4}{(p^2)^2} + \frac{169}{90}\frac{(p_\mu^2 + p_\nu^2)}{p^2}\right)\right]\right\} \\ &+ \mathcal{O}(a^4, g^4) \end{aligned} \quad (38)$$

$$\begin{aligned} \text{Tr}\left[L^{\text{DA1}}(p) \cdot L_{\text{tree}}^{\text{DA1}}(p)\right] &= 2p_\mu^2 + \frac{1}{4}p^2 + \textcolor{red}{a}^2\left(-\frac{1}{12}p^4 - \frac{2}{3}p_\mu^4\right) \\ &+ \tilde{g}^2\left\{-\frac{4}{3}\frac{p_\mu^4}{p^2} + p^2\left(-4.127332(3) + \frac{2}{3}\ln(\textcolor{red}{a}^2 p^2)\right) + p_\mu^2\left(-31.68532(3) + \frac{16}{3}\ln(\textcolor{red}{a}^2 p^2)\right) \right. \\ &\quad + \textcolor{red}{a}^2\left[(p^2)^2\left(0.17035(2) + \frac{65}{288}\ln(\textcolor{red}{a}^2 p^2)\right) + p^2 p_\mu^2\left(0.3982(1) - \frac{541}{180}\ln(\textcolor{red}{a}^2 p^2)\right) \right. \\ &\quad \left. + p^4\left(1.69230(3) - \frac{397}{720}\ln(\textcolor{red}{a}^2 p^2) + \frac{43}{360}\frac{p_\mu^2}{p^2}\right) \right. \\ &\quad \left. \left. + p_\mu^4\left(18.4613(5) + \frac{2}{5}\ln(\textcolor{red}{a}^2 p^2) - \frac{29}{90}\frac{p^4}{(p^2)^2} - \frac{169}{45}\frac{p_\mu^2}{p^2}\right)\right]\right\} \\ &+ \mathcal{O}(a^4, g^4) \end{aligned} \quad (39)$$

$$\begin{aligned}
\text{Tr} \left[L^{\text{DA2}}(p) \cdot L_{\text{tree}}^{\text{DA2}}(p) \right] &= p_\mu^2 + p_\nu^2 - \frac{a^2}{3} (p_\mu^4 + p_\nu^4) \\
&+ \tilde{g}^2 \left\{ -\frac{4}{3} \frac{p_\mu^2 p_\nu^2}{p^2} + (p_\mu^2 + p_\nu^2) \left(-16.10196(1) + \frac{8}{3} \ln(a^2 p^2) \right) \right. \\
&\quad + a^2 \left[(p_\mu^4 + p_\nu^4) \left(7.2286(1) - \frac{491}{360} \ln(a^2 p^2) \right) \right. \\
&\quad \quad + (p_\mu^2 + p_\nu^2) \left(p^2 \left(0.75869(3) - \frac{137}{360} \ln(a^2 p^2) \right) - \frac{353}{720} \frac{p^4}{p^2} \right) \\
&\quad \quad \left. \left. + p_\mu^2 p_\nu^2 \left(4.8509(1) + \frac{187}{180} \ln(a^2 p^2) - \frac{29}{90} \frac{p^4}{(p^2)^2} - \frac{169}{90} \frac{(p_\mu^2 + p_\nu^2)}{p^2} \right) \right] \right\} \\
&+ \mathcal{O}(a^4, g^4)
\end{aligned} \tag{40}$$

$$\begin{aligned}
\text{Tr} \left[L^{\text{DT1}}(p) \cdot L_{\text{tree}}^{\text{DT1}}(p) \right] &= \frac{p^2 - p_\mu^2}{4} + 2p_\nu^2 + a^2 \left(\frac{p_\mu^4 - p^4}{12} - \frac{2p_\nu^4}{3} \right) \\
&+ \tilde{g}^2 \left\{ (p_\mu^2 - p^2) \left(4.226559(3) - \ln(a^2 p^2) \right) + p_\nu^2 \left(-29.11666(2) + 5 \ln(a^2 p^2) \right) \right. \\
&\quad + a^2 \left[p^4 \left(-0.14754(2) - \frac{43}{1440} \ln(a^2 p^2) \right) \right. \\
&\quad + p^4 \left(1.93789(3) - \frac{433}{720} \ln(a^2 p^2) - \frac{379}{720} \frac{p_\nu^2}{p^2} + \frac{17}{192} \frac{p_\mu^2}{p^2} \right) \\
&\quad + p^2 \left(1.7215(1) p_\nu^2 + \frac{61}{48} \ln(a^2 p^2) p_\nu^2 + 0.37022(2) p_\mu^2 - \frac{227}{1440} \ln(a^2 p^2) p_\mu^2 \right) \\
&\quad + p_\nu^4 \left(14.9155(4) - \frac{71}{15} \ln(a^2 p^2) - \frac{721}{90} \frac{p_\mu^2}{p^2} \right) \\
&\quad + p_\nu^2 p_\mu^2 \left(2.4896(1) - \frac{881}{240} \ln(a^2 p^2) - \frac{39}{10} \frac{p_\mu^2}{p^2} \right) \\
&\quad \left. \left. + p_\mu^4 \left(-2.24911(4) + \frac{71}{90} \ln(a^2 p^2) \right) - \frac{134}{45} \frac{p_\nu^6}{p^2} \right] \right\} \\
&+ \mathcal{O}(a^4, g^4)
\end{aligned} \tag{41}$$

$$\begin{aligned}
\text{Tr} \left[L^{\text{DT2}}(p) \cdot L_{\text{tree}}^{\text{DT2}}(p) \right] &= p_\rho^2 + p_\nu^2 + a^2 \left(-\frac{p_\rho^4}{3} - \frac{p_\nu^4}{3} \right) \\
&+ \tilde{g}^2 \left\{ (p_\nu^2 + p_\rho^2) \left(-15.84740(1) + 3 \ln(a^2 p^2) \right) \right. \\
&\quad + a^2 \left[(p_\nu^2 + p_\rho^2) \left(0.22134(3) p^2 + \frac{107}{360} \ln(a^2 p^2) p^2 - \frac{41}{60} \frac{p^4}{p^2} \right) \right. \\
&\quad \quad + 0.73604(2) p_\mu^2 - \frac{301}{360} \ln(a^2 p^2) p_\mu^2 - \frac{67}{90} \frac{p_\mu^4}{p^2} \\
&\quad \quad - \frac{67}{15} \frac{p_\rho^2 p_\mu^2 p_\nu^2}{p^2} + (p_\nu^4 + p_\rho^4) \left(7.3949(1) - \frac{1051}{720} \ln(a^2 p^2) \right) \\
&\quad \quad \left. \left. + p_\rho^2 p_\nu^2 \left(2.98450(8) - \frac{1609}{360} \ln(a^2 p^2) \right) - \frac{67}{45} \frac{p_\rho^4 p_\nu^2 + p_\rho^2 p_\nu^4}{p^2} \right] \right\} \\
&+ \mathcal{O}(a^4, g^4)
\end{aligned} \tag{42}$$

In our forthcoming publication [13], we will include an ASCII file with all our numerical results for general value of λ , c_{sw} , m_0 and the 10 sets of Symanzik gluon actions; the file is best perused as Mathematica input. In addition, there appears an Appendix providing the exact $\mathcal{O}(a^2)$ terms that need to be subtracted from Z_O (a fraction of the two traces and Z_q of Eq. (28)).

The $\mathcal{O}(a^2)$ terms shown in Eqs. (37) - (40) are used to correct our non-perturbative results for Z_{DV1} , Z_{DV2} , Z_{DA1} , Z_{DA2} , in order to better control a^2 artifacts. For the subtraction procedure we use the boosted coupling [16] instead of the bare one

$$g_{\text{boosted}}^2 = \frac{g_{\text{bare}}^2}{\langle u_{\text{plaq}} \rangle}, \tag{43}$$

where $\langle u_{\text{plaq}} \rangle$ is the plaquette mean value.

IV. NON-PERTURBATIVE CALCULATION

A. Evaluation of correlators

In the literature there are two main approaches that have been employed for the non-perturbative evaluation of the renormalization constants. They both start by considering that the operators can all be written in the form

$$\mathcal{O}(z) = \sum_{z'} \bar{u}(z) \mathcal{J}(z, z') d(z'), \quad (44)$$

where u and d denote quark fields in the physical basis and \mathcal{J} denotes the operator we are interested in, e.g. $\mathcal{J}(z, z') = \delta_{z, z'} \gamma_\mu$ would correspond to the local vector current. For each operator we define a bare vertex function given by

$$G(p) = \frac{a^{12}}{V} \sum_{x, y, z, z'} e^{-ip(x-y)} \langle u(x) \bar{u}(z) \mathcal{J}(z, z') d(z') \bar{d}(y) \rangle, \quad (45)$$

where p is a momentum allowed by the boundary conditions, V is the lattice volume, and the gauge average is performed over gauge-fixed configurations. We have suppressed the Dirac and color indices of $G(p)$. The first approach relies on translation invariance to shift the coordinates of the correlators in Eq. (45) to position $z = 0$ [17, 18]. Having shifted to $z = 0$ allows one to calculate the amputated vertex function for a given operator \mathcal{J} for *any* momentum with one inversion per quark flavor.

In this work we explore the second approach, introduced in Ref. [19], which uses directly Eq. (45) without employing translation invariance. One must now use a source that is momentum dependent but can couple to any operator. For twisted mass fermions, we use the symmetry $S^u(x, y) = \gamma_5 S^{d\dagger}(y, x) \gamma_5$ between the u - and d -quark propagators. Therefore with a single inversion one can extract the vertex function for a *single* momentum. The advantage of this approach is a high statistical accuracy and the evaluation of the vertex for any operator including extended operators at no significant additional computational cost. Since we are interested in a number of operators with their associated renormalization constants we use the second approach. We fix to Landau gauge using a stochastic over-relaxation algorithm [20], converging to a gauge transformation which minimizes the functional

$$F = \sum_{x, \mu} \text{Re tr} [U_\mu(x) + U_\mu^\dagger(x - \hat{\mu})]. \quad (46)$$

Questions related to the Gribov ambiguity will not be addressed in this work. The propagator in momentum space, in the physical basis, is defined by

$$S^u(p) = \frac{a^8}{V} \sum_{x, y} e^{-ip(x-y)} \langle u(x) \bar{u}(y) \rangle, \quad S^d(p) = \frac{a^8}{V} \sum_{x, y} e^{-ip(x-y)} \langle d(x) \bar{d}(y) \rangle. \quad (47)$$

An amputated vertex function is given by

$$\Gamma(p) = (S^u(p))^{-1} G(p) (S^d(p))^{-1}. \quad (48)$$

and the corresponding renormalized quantities are

$$S_R(p) = Z_q S(p), \quad \Gamma_R(p) = Z_q^{-1} Z_O \Gamma(p), \quad (49)$$

In the twisted basis at maximal twist, Eq. (45) takes the form

$$G(p) = \frac{a^{12}}{4V} \sum_{x, y, z, z'} e^{-ip(x-y)} \langle (\mathbb{1} + i\gamma_5) u(x) \bar{u}(z) (\mathbb{1} + i\gamma_5) \mathcal{J}(z, z') (\mathbb{1} - i\gamma_5) d(z') \bar{d}(y) (\mathbb{1} - i\gamma_5) \rangle. \quad (50)$$

After integration over the fermion fields, and using $S^u(x, z) = \gamma_5 \mathcal{S}^{d\dagger}(z, x) \gamma_5$ this becomes

$$G(p) = \frac{a^{12}}{4V} \sum_z \left\langle (\mathbb{1} - i\gamma_5) \check{\mathcal{S}}^{d\dagger}(z, p) (\mathbb{1} - i\gamma_5) \mathcal{J}(z, z') (\mathbb{1} - i\gamma_5) \check{\mathcal{S}}^d(z, p) (\mathbb{1} - i\gamma_5) \right\rangle^G, \quad (51)$$

where $\langle \dots \rangle^G$ is the integration over gluon fields, and $\check{\mathcal{S}}(z, p) = \sum_y e^{ipy} \mathcal{S}(z, y)$ is the Fourier transformed propagator on one of its argument on a particular gauge background. It can be obtained by inversion using the Fourier source

$$b_\alpha^a(x) = e^{ipx} \delta_{\alpha\beta} \delta_{ab}, \quad (52)$$

for all Dirac α and color a indices. The propagators in the physical basis given in Eq. (47) can be obtained from

$$\begin{aligned} S^d(p) &= \frac{1}{4} \sum_z e^{-ipz} \langle (\mathbb{1} - i\gamma_5) \check{S}^d(z, p) (\mathbb{1} - i\gamma_5) \rangle^G \\ S^u(p) &= -\frac{1}{4} \sum_z e^{+ipz} \langle (\mathbb{1} - i\gamma_5) \check{S}^{d\dagger}(z, p) (\mathbb{1} - i\gamma_5) \rangle^G, \end{aligned} \quad (53)$$

which evidently only need 12 inversions despite the occurrence of both u and d quarks in the original expression.

We evaluate Eq. (50) and Eq. (53) for each momentum separately employing Fourier sources over a range of $a^2 p^2$ for which perturbative results can be trusted and finite a corrections are reasonably small.

B. Renormalization Condition

The renormalization constants are computed both perturbatively and non-perturbatively in the RI'-MOM scheme at different renormalization scales. We translate them to the $\overline{\text{MS}}$ -scheme at $(2 \text{ GeV})^2$ using a conversion factor computed in perturbation theory to $\mathcal{O}(g^6)$ as described in Section V. The Z-factors are determined by imposing the following conditions:

$$Z_q = \frac{1}{12} \text{Tr} \left[(S^L(p))^{-1} S^{(0)}(p) \right] \Big|_{p^2=\mu^2} \quad (54)$$

$$Z_q^{-1} Z_{\mathcal{O}}^{\mu\nu} \frac{1}{12} \text{Tr} \left[\Gamma_{\mu\nu}^L(p) \Gamma_{\mu\nu}^{(0)-1}(p) \right] \Big|_{p^2=\mu^2} = 1, \quad (55)$$

where μ is the renormalization scale, while S_L and Γ_L correspond to the perturbative or non-perturbative results. The trace is now taken over spin and color indices. These conditions are imposed in the massless theory, i.e. at critical mass and vanishing twisted mass. At finite lattice spacing there are two choices for $S^{(0)}$ and $\Gamma^{(0)}$ entering Eq. (55). One can take either the tree level or the continuum results for $S^{(0)}$ and $\Gamma^{(0)}$, which differ by $\mathcal{O}(a^2)$ -terms. The continuum free propagator in terms of continuum momentum is

$$S^{(0)}(p) = \frac{-i \sum_{\rho} \gamma_{\rho} p_{\rho}}{p^2} \quad (56)$$

$$\Gamma_{\mu\nu}^{(0)}(p) = -i \tilde{\mathcal{O}}_{\{\mu} p_{\nu\}}. \quad (57)$$

We refer to this choice as *method 1*. A different choice is to define the free propagator using the lattice momentum [18, 19] :

$$S^{(0)}(p) = \frac{-i \sum_{\rho} \gamma_{\rho} \sin(p_{\rho})}{\sum_{\rho} \sin(p_{\rho})^2} \quad (58)$$

$$\Gamma_{\mu\nu}^{(0)}(p) = -i \tilde{\mathcal{O}}_{\{\mu} \sin(p_{\nu\}}), \quad (59)$$

which we will refer to as *method 2* used in Ref. [21].

The choices for $S^{(0)}$ and $\Gamma_{\mu\nu}^{(0)}$ given in Eqs. (58) - (59) are preferable, compared to Eqs. (56) - (57), since only for method 2 we obtain $Z_q = 1$, $Z_{\mathcal{O}} = 1$ when the gauge field is set to unity. Similarly, in the perturbative computation only method 2 gives $Z_q = 1$, and $Z_{\mathcal{O}} = 1$ at tree-level. On the contrary, the Z-factors obtained from method 1 have lattice artifacts even at tree-level. In this sense, method 2 is an improvement of method 1, and can be thus considered superior. Obviously, the renormalization constants using the two methods differ only in their lattice artifacts, as can be seen by Eq. (23). We find that, for the cases considered here, non-perturbative results using method 2 lead to Z-factors with smaller lattice effects. We demonstrate this by examining the following case: Let us consider the momenta as given in Table II, which fall into two sets, those with spatial components $2\pi(2, 2, 2)/L$ and those with $2\pi(3, 3, 3)/L$; there is only one non democratic momentum, with spatial components $2\pi(3, 3, 2)/L$, but this behaves similarly to the second set mentioned above. The two sets of momenta do not fall on the same curve, a behavior that is due to cut-off effects. This is clearly seen in Fig. 3 where we present $Z_{\text{DA}}^{0\nu}$ at $\beta = 3.9$ and $\mu_0 = 0.0085$ using the two methods (upper plot) (similarly for $Z_{\text{DV}}^{0\nu}$ in Fig. 4). The statistical errors in Fig. 3 and the rest of the graphs are smaller than the size of the symbols. As can be seen, the two sets of momenta differ in particular when using method

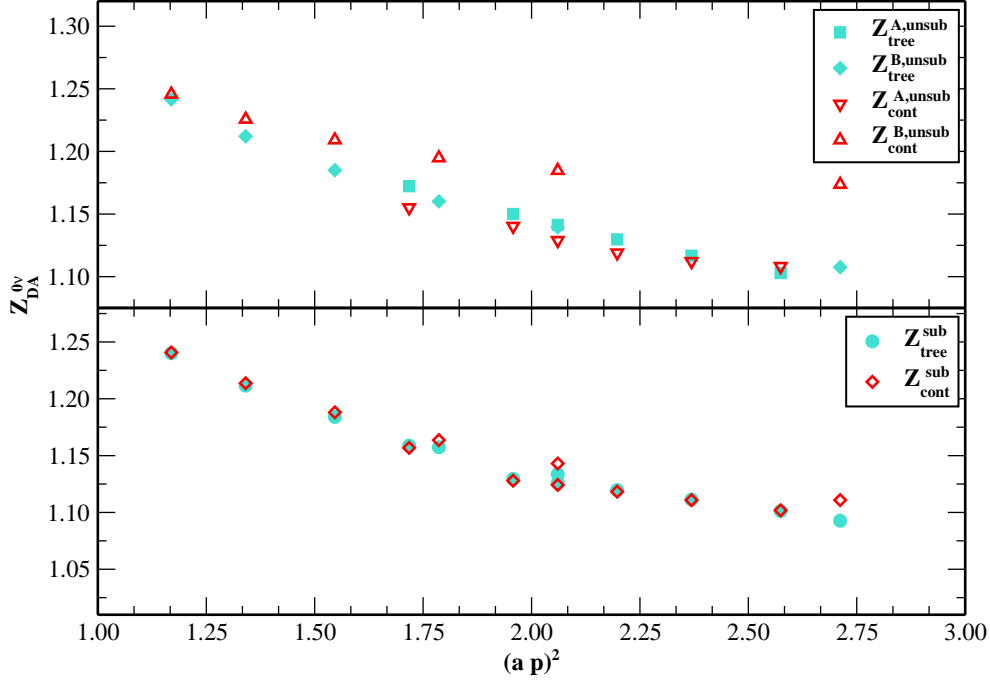


FIG. 3: $Z_{DA}^{0\nu}$ for $\beta = 3.9$ ($a^{-1}=2.217$ GeV) and $m_\pi = 0.430$ GeV for method 1 (open symbols) and method 2 (filled symbols). The upper plot corresponds to non-perturbative results, where the index A, B represents the set of momenta with spatial components $2\pi/L(3,3,3)$ and $2\pi/L(2,2,2)$, respectively. The lower plot shows the non-perturbative results after subtracting the perturbative $\mathcal{O}(g^2 a^2)$ -terms, where the two methods give almost identical results. Moreover, in method 1, the jump between the two sets of momenta disappears.

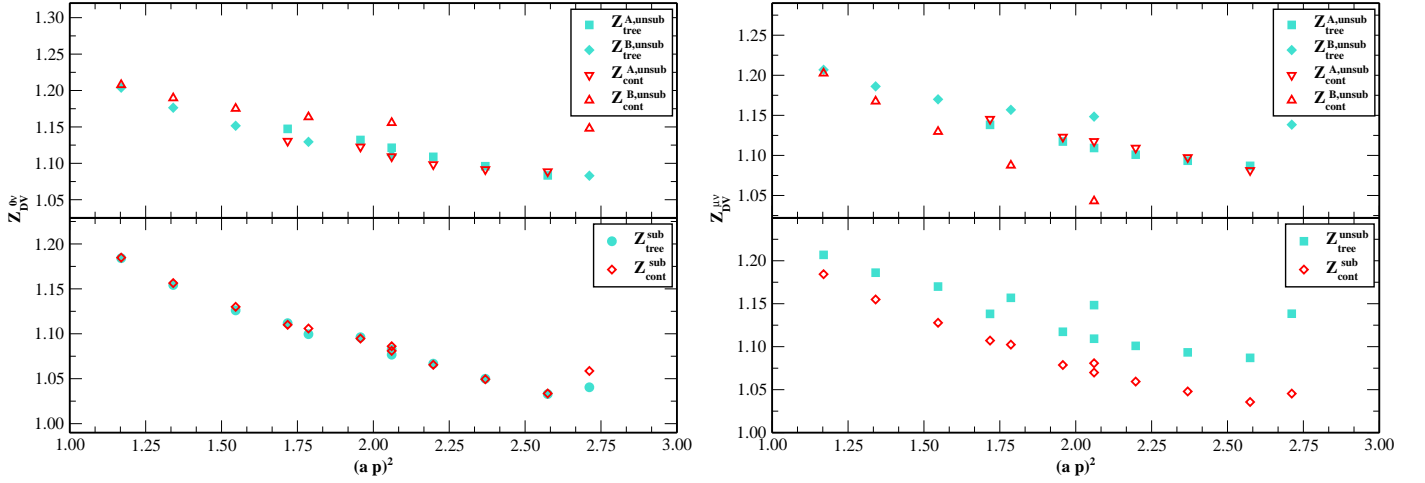


FIG. 4: In the left panel we show $Z_{DV}^{0\nu}$ using the same notation as in Fig. 3. In the right panel, upper graph we show $Z_{DV}^{\mu\nu}$ again using the notation of Fig.3 whereas in the lower graph we show a comparison between method 1 after subtracting the perturbative $\mathcal{O}(a^2)$ -terms (diamonds) and method 2 without any subtractions (filled squares).

1. However, it is important to note that, after subtracting the $\mathcal{O}(a^2)$ perturbative contributions one obtains values that are consistent between the two methods (see lower plot). Moreover, in method 1 the jump observed between the two sets of momenta disappears. For method 1 the subtraction of the perturbative $\mathcal{O}(a^2)$ terms refers to both contributions of $\mathcal{O}(g^0 a^2)$ (tree-level) and $\mathcal{O}(g^2 a^2)$ (1-loop). Thus, *upon subtraction* method 1 can be compared to method 2 because we remove all $\mathcal{O}(a^2)$ terms up to 1-loop, leading to almost equivalent results as can be seen in the lower plot in Fig. 3. We would like to stress that the subtraction is necessary and yields results superior to using the unsubtracted method 2. This is demonstrated in Fig. 4 in the right hand side plots where in the upper plot we

show the unsubtracted methods 1 and 2, while in the lower plot we show a comparison method 1 after subtraction of perturbative $\mathcal{O}(a^2)$ -terms with the unsubtracted method 2. One can observe that the jump between different set of momenta, appearing in the unsubtracted method 2, almost disappears in the subtracted method 1. The same pattern appears in all Z-factors of the one-derivative operators, as well as for Z_q . The latter has an impact on all other renormalization constants discussed here. This effect, as expected, becomes less pronounced at $\beta = 4.05$ and 4.20 , and disappears for small $a^2 p^2$ as demonstrated in the next section. The results presented in all Tables correspond to the Z-factors obtained using method 2.

V. RESULTS

A. RI'-MOM condition

We perform the calculation of renormalization constants for three values of the lattice spacing corresponding to $\beta = 3.9$, 4.05 and 4.20 . The lattice spacing as determined from the nucleon mass is 0.089 fm, 0.070 fm and 0.056 fm respectively. For $\beta = 3.9$ we consider three different quark masses, corresponding to $m_\pi = 0.302$ GeV ($a\mu_0 = 0.004$), $m_\pi = 0.376$ GeV ($a\mu_0 = 0.0064$) and $m_\pi = 0.430$ GeV ($a\mu_0 = 0.0085$), in order to explore the dependence of the Z-factors on the pion mass. At $\beta = 4.05$ we consider two volumes, $24^3 \times 48$ and $32^3 \times 64$ in order to check for finite volume effects. To extract the renormalization constants reliably one needs to consider momenta in the range $\Lambda_{QCD} < p < 1/a$. We relax the upper bound to be $\sim 2/a$ to $3/a$, which is justified by the linear dependence of our results on a^2 . Therefore, for each value of β we consider momenta spanning the range $1 < a^2 p^2 < 2.7$ for which perturbation theory is trustworthy and lattice artifacts are still small enough. In Table I we summarize the various parameters of the action, that we used in our simulations.

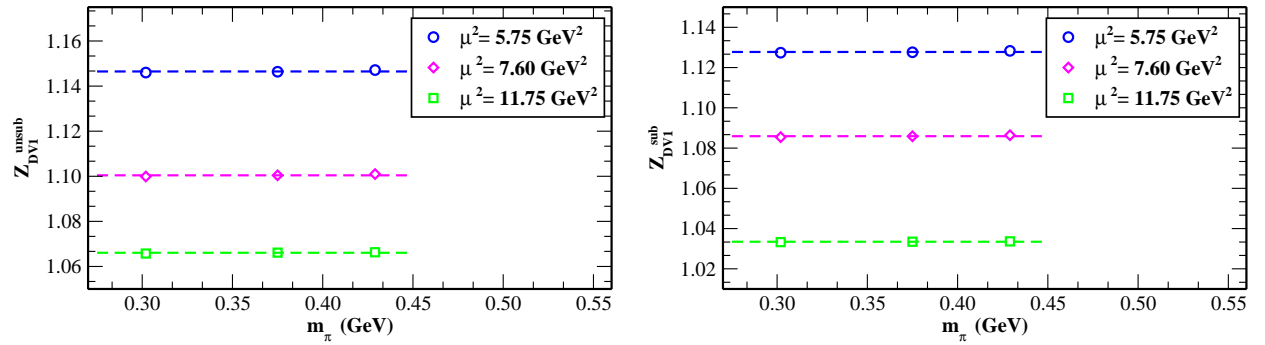
β	a (fm)	$a\mu_0$	m_π (GeV)	$L^3 \times T$
3.9	0.089	0.0040	0.3021(14)	$24^3 \times 48$
3.9	0.089	0.0064	0.37553(80)	$24^3 \times 48$
3.9	0.089	0.0085	0.4302(11)	$24^3 \times 48$
4.05	0.070	0.006	0.4082(31)	$24^3 \times 48$
4.05	0.070	0.006	0.404(2)	$32^3 \times 64$
4.05	0.070	0.008	0.465(1)	$32^3 \times 64$
4.20	0.055	0.0065	0.476(2)	$32^3 \times 64$

TABLE I: Action parameters used in the simulations.

In Table II we present the statistical sample for the parameters and momenta we used in the simulations. Using the number of configurations shown in Table II leads to results with very high statistical accuracy, easily below 0.5%. The results for the subtracted Z-factors (method 2) at $\beta = 3.9$ are tabulated in Table III for the highest and lowest twisted mass parameter used (for the lowest mass we have obtained the Z-factors only for 6 momenta). Comparison between the Z-factors for two different masses shows that any dependence on the pion mass is within the small statistical errors. This negligible dependence is not a result of the $\mathcal{O}(a^2)$ subtraction, as demonstrated in Fig. 5. The left plot illustrates the pion mass dependence of the unsubtracted Z_{DV1} for three renormalization scales ranging from 5.75 GeV² to 11.75 GeV², while the subtracted Z_{DV1} is shown in the right plot. The same behavior is observed for all renormalization constants considered here. The subtracted Z-factors (method 2) for $\beta = 4.05$ and $\beta = 4.20$ are presented in Tables IV-V, respectively. In order to see possible volume effects we compute the renormalization constants at $\beta = 4.05$, $\mu_0 = 0.006$, for two lattices with different size, namely for $24^3 \times 48$ and for $32^3 \times 64$. For this comparison we used momenta that correspond to the same renormalization scale: For the small lattice we use $2\pi(3/48, 3/24, 3/24, 3/24)$, in lattice units, whereas for the larger one we employ $2\pi(4/64, 4/32, 4/32, 4/32)$. The volume effects appear to be $\sim 0.1\%$, as can be seen from Table VI.

Given the small statistical errors one may carefully examine the systematic errors. As already noted a systematic effect comes from the choice of $S^{(0)}$ and $\Gamma^{(0)}$. To give an example, at $\beta = 3.9$, $\mu_0 = 0.004$, $\mu^2 \approx 5.75$ GeV² method 1 leads to $Z_q = 0.76606(7)$ while method 2 gives $Z_q = 0.80514(7)$, before any subtraction of $\mathcal{O}(a^2)$ is carried out. This systematic effect is removed after perturbative subtraction is applied. Another, much smaller, systematic effect comes from the asymmetry of our lattices both because they are larger in their time extent and because of the antiperiodic

(n_t, n_x, n_y, n_z)	$\beta = 3.9$ $24^3 \times 48$ $\mu_0 = 0.004$	$\beta = 3.9$ $24^3 \times 48$ $\mu_0 = 0.0064$	$\beta = 3.9$ $24^3 \times 48$ $\mu_0 = 0.0085$	$\beta = 4.05$ $24^3 \times 48$ $\mu_0 = 0.006$	$\beta = 4.05$ $32^3 \times 64$ $\mu_0 = 0.006$	$\beta = 4.05$ $32^3 \times 64$ $\mu_0 = 0.008$	$\beta = 4.20$ $32^3 \times 64$ $\mu_0 = 0.0065$
(4,2,2,2)	100	50	80	—	50	50	15
(5,2,2,2)	100	60	60	—	—	33	15
(6,2,2,2)	100	50	50	—	—	50	15
(3,3,3,2)	—	—	27	—	—	15	15
(7,2,2,2)	—	—	20	—	—	15	15
(2,3,3,3)	—	—	20	—	—	15	15
(8,2,2,2)	—	—	20	—	—	15	15
(3,3,3,3)	100	50	80	15	—	50	15
(4,4,4,4)	—	—	—	—	15	—	—
(4,3,3,3)	100	60	60	—	—	50	15
(5,3,3,3)	100	60	60	—	—	50	15
(6,3,3,3)	—	—	15	—	—	15	15
(10,2,2,2)	—	—	15	—	—	15	15
(8,3,3,3)	—	—	—	—	—	15	15
(9,3,3,3)	—	—	—	—	—	15	15
(10,3,3,3)	—	—	—	—	—	15	15
(13,2,2,2)	—	—	—	—	—	15	15
(11,3,3,3)	—	—	—	—	—	15	15
(14,2,2,2)	—	—	—	—	—	15	15
(7,4,4,4)	—	—	15	—	—	—	—
(8,4,4,4)	—	—	15	—	—	15	—
(9,4,4,4)	—	—	15	—	—	15	—
(10,4,4,4)	—	—	—	—	—	15	—
(11,2,2,2)	—	—	15	—	—	—	—
(12,2,2,2)	—	—	15	—	—	—	—
(12,3,3,3)	—	—	15	—	—	—	—
(13,3,3,3)	—	—	—	—	—	15	—
(14,3,3,3)	—	—	—	—	—	15	—

TABLE II: Statistical sample at $\beta = 3.9, 4.05, 4.20$ for various momenta.FIG. 5: Z_{DV1} at $\beta = 3.9$, as a function of the pion mass: $m_\pi = 0.302$ GeV ($a\mu_0 = 0.004$), $m_\pi = 0.375$ GeV ($a\mu_0 = 0.0064$) and $m_\pi = 0.429$ GeV ($a\mu_0 = 0.0085$). The left plot regards the unsubtracted non-perturbative results and the right one corresponds to the subtracted data.

boundary conditions in the time direction. For instance, using the same β and μ_0 as in the previous example, method 1 at $\mu^2 \approx 7.6$ GeV², in the temporal direction of the current gives $Z_{DV1} = 1.1387(2)$ while the average from the three spatial directions leads to $Z_{DV1} = 1.1006(2)$. This effect can be seen in Fig. 6 where we plot separately the renormalization constant Z_{DV1} determined from the temporal indices, the spatial indices and the average of those two. In the same figure we also show that upon subtraction this systematic effect disappears (lower plot). For Tables III - V we use for Z_{DV1} the average of Z_{DV}^{00} , $Z_{DV}^{\nu\nu}$ with $\nu = 1, 2, 3$, while for Z_{DV2} the average of $Z_{DV}^{0\nu}$, $Z_{DV}^{\nu\rho}$ with $\nu \neq \rho = 1, 2, 3$. We apply the same procedure for the twist-2 axial operator.

Chiral extrapolations are necessary to obtain the renormalization factors in the chiral limit. As already pointed out

$\mu_0 = 0.004$					$\mu_0 = 0.0085$				
(n_t, n_x, n_y, n_z)	Z_{DV1}	Z_{DV2}	Z_{DA1}	Z_{DA2}	Z_{DV1}	Z_{DV2}	Z_{DA1}	Z_{DA2}	
(4,2,2,2)	1.1274(1)	1.1836(4)	1.2044(2)	1.2387(4)	1.1283(2)	1.1846(5)	1.2051(2)	1.2395(5)	
(5,2,2,2)	1.1058(1)	1.1548(4)	1.1792(2)	1.2094(4)	1.1067(2)	1.1558(5)	1.1800(2)	1.2102(5)	
(6,2,2,2)	1.0854(1)	1.1283(3)	1.1567(2)	1.1820(3)	1.0864(1)	1.1291(4)	1.1576(2)	1.1829(4)	
(3,3,3,2)	—	—	—	—	1.0740(1)	1.1088(4)	1.1418(2)	1.1626(4)	
(7,2,2,2)	—	—	—	—	1.06613(8)	1.1042(4)	1.1363(2)	1.1568(4)	
(2,3,3,3)	—	—	—	—	1.0587(1)	1.0869(4)	1.1331(2)	1.1391(4)	
(8,2,2,2)	—	—	—	—	1.04684(6)	1.0830(3)	1.1176(1)	1.1341(3)	
(3,3,3,3)	—	—	—	—	1.05045(6)	1.0756(2)	1.11066(9)	1.1321(2)	
(4,3,3,3)	1.04985(7)	1.0750(3)	1.1100(1)	1.1315(3)	1.04204(6)	1.0625(2)	1.09097(9)	1.1229(2)	
(5,3,3,3)	1.04152(6)	1.0620(2)	1.09035(9)	1.1223(2)	1.03367(6)	1.0487(2)	1.07377(9)	1.1124(2)	
(6,3,3,3)	1.03327(5)	1.0482(2)	1.07332(8)	1.1120(2)	1.02513(5)	1.0346(2)	1.05817(6)	1.1009(1)	
(10,2,2,2)	—	—	—	—	1.00804(9)	1.0482(2)	1.08561(9)	1.0945(2)	

TABLE III: The renormalization constants at $\beta = 3.9$ with $\mu_0 = 0.004, 0.0085$ for lattice size: $24^3 \times 48$.

(n_t, n_x, n_y, n_z)	Z_{DV1}	Z_{DV2}	Z_{DA1}	Z_{DA2}
(4,2,2,2)	1.1960(1)	1.2644(3)	1.2749(1)	1.3126(3)
(5,2,2,2)	1.1718(2)	1.2324(5)	1.2483(2)	1.2794(5)
(6,2,2,2)	1.1491(1)	1.2016(2)	1.2244(1)	1.2475(2)
(3,3,3,2)	1.1336(1)	1.1805(3)	1.2069(1)	1.2260(3)
(7,2,2,2)	1.1280(2)	1.1745(2)	1.2025(2)	1.2200(2)
(2,3,3,3)	1.1188(1)	1.1555(3)	1.1948(1)	1.1998(3)
(8,2,2,2)	1.1086(1)	1.1493(2)	1.1826(2)	1.1931(2)
(3,3,3,3)	1.10592(6)	1.1458(1)	1.17497(7)	1.1914(2)
(4,3,3,3)	1.09370(5)	1.1339(1)	1.15739(6)	1.1807(1)
(5,3,3,3)	1.08232(5)	1.1206(1)	1.14186(6)	1.1683(1)
(6,3,3,3)	1.07144(9)	1.1068(2)	1.1278(1)	1.1551(2)
(10,2,2,2)	1.0724(1)	1.1090(2)	1.1477(1)	1.1505(2)

TABLE IV: Renormalization constants at $\beta = 4.05, a\mu_0 = 0.008$ for lattice size $32^3 \times 64$.

the dependence on the pion mass is insignificant. Allowing a slope and performing a linear extrapolation to the data shown in Fig. 5 yields a slope consistent with zero. This behavior is also observed at the other β -values and therefore the renormalization constants are computed at one quark mass, given in the Tables III-V. Figures 7, 8, 9 demonstrate the effect of subtraction, for all three β values, as a function of the renormalization scale (in lattice units). For all cases we observe a significant correction upon subtraction; the lattice artifacts for Z_{DA2} turn out to be very small for most values of the momentum. In addition, the lattice artifacts decrease by employing higher values for β (finer lattice), as expected.

B. RI'-MOM at a reference scale

All our Z-factors have been evaluated for a range of renormalization scales. In this subsection we use 2-loop perturbative expressions to extrapolate to a scale $\mu = 1/a$ (the values for a are taken from Table I). Thus, each result is extrapolated to $1/a$, maintaining the information of the initial renormalization scale at which it was computed. Although the 3-loop formula is available for the following expressions, the $\mathcal{O}(g^6)$ corrections are insignificant compared to the lower order results.

The scale dependence is predicted by the renormalization group (at fixed bare parameters), that is

$$Z_O^{\text{RI}'}(\mu) = R_O(\mu, \mu_0) Z_O^{\text{RI}'}(\mu_0) \quad (60)$$

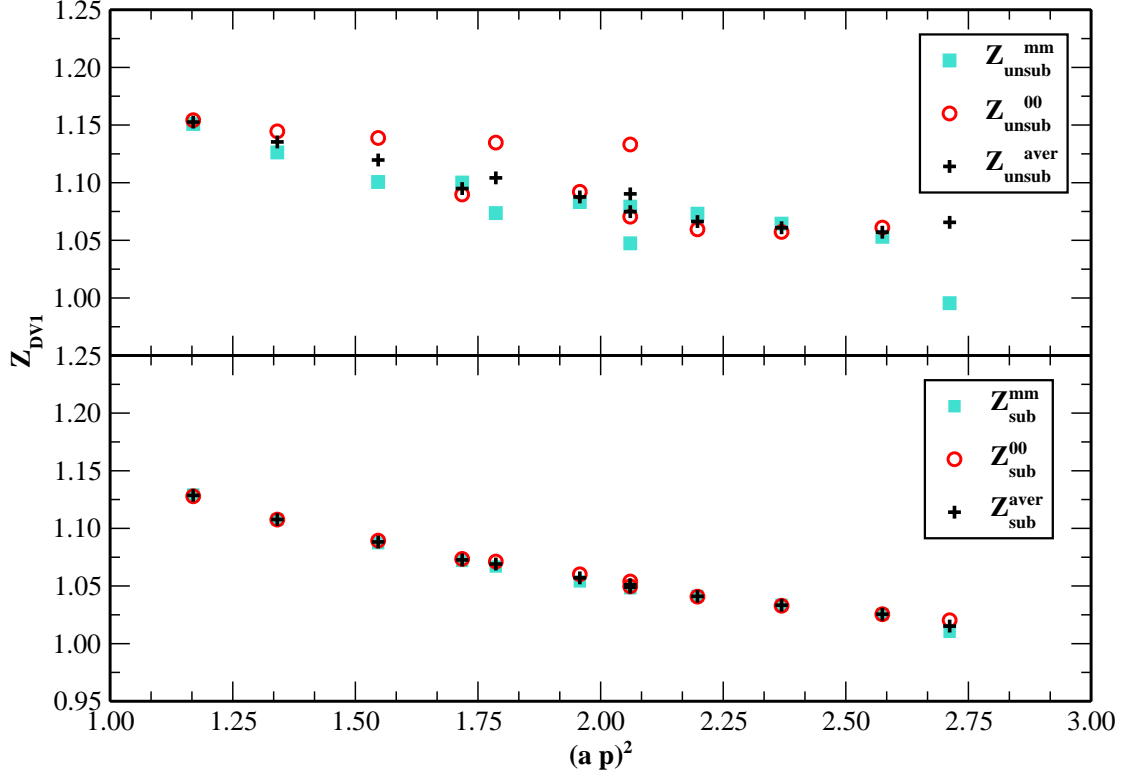


FIG. 6: $Z_{DV}^{\mu\mu}$ (squares), Z_{DV}^{00} (circles), Z_{DV}^{aver} (crosses), for $\beta = 3.9$ ($a^{-1}=2.217$ GeV), $m_\pi = 0.430$ GeV using method 1. The upper plot corresponds to the purely non-perturbative results, while the lower plot shows the non-perturbative results after subtracting the perturbative terms of $\mathcal{O}(a^2)$.

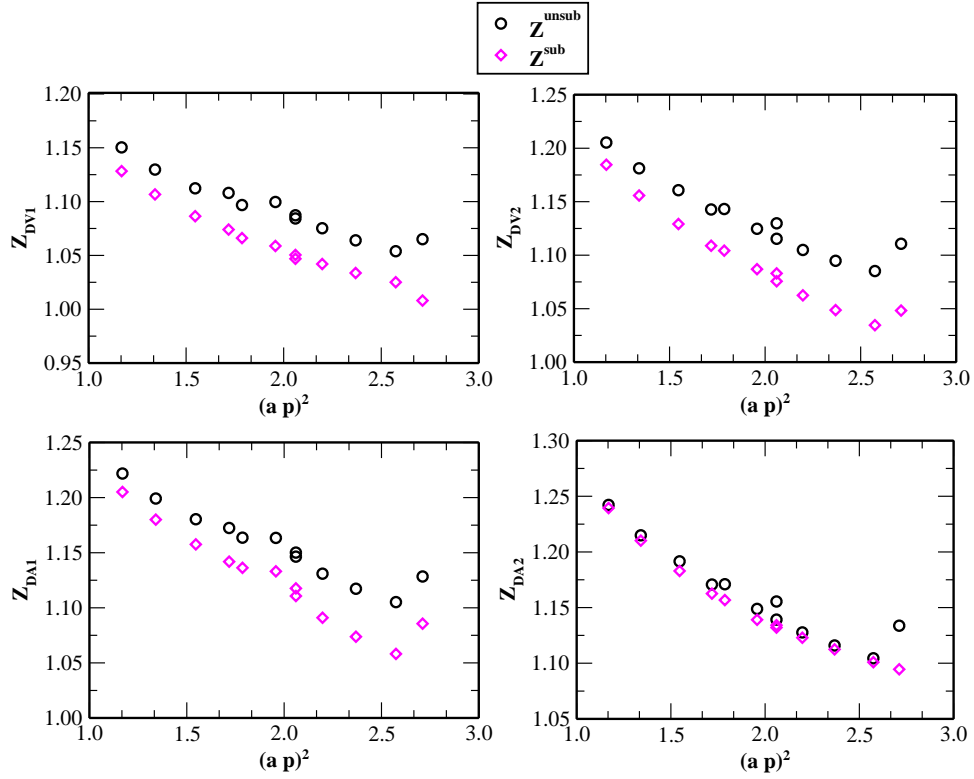


FIG. 7: Renormalization scale dependence for the Z-factors at $\beta = 3.9$ and $m_\pi = 0.430$ GeV

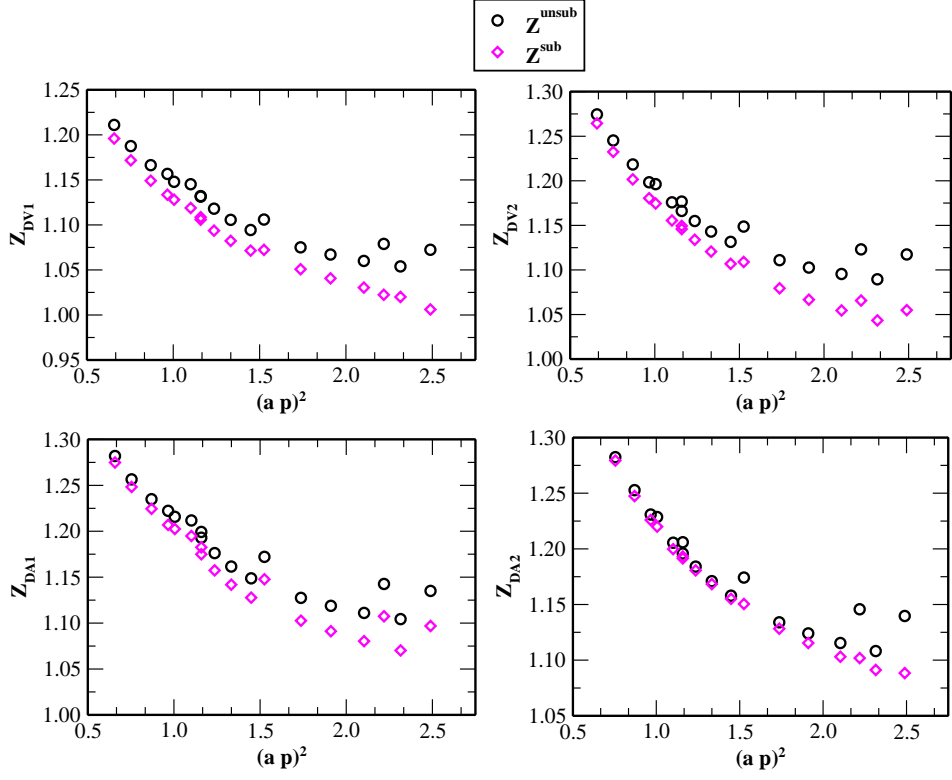


FIG. 8: Renormalization scale dependence for the Z-factors at $\beta = 4.05$ and $m_\pi = 0.465$ GeV

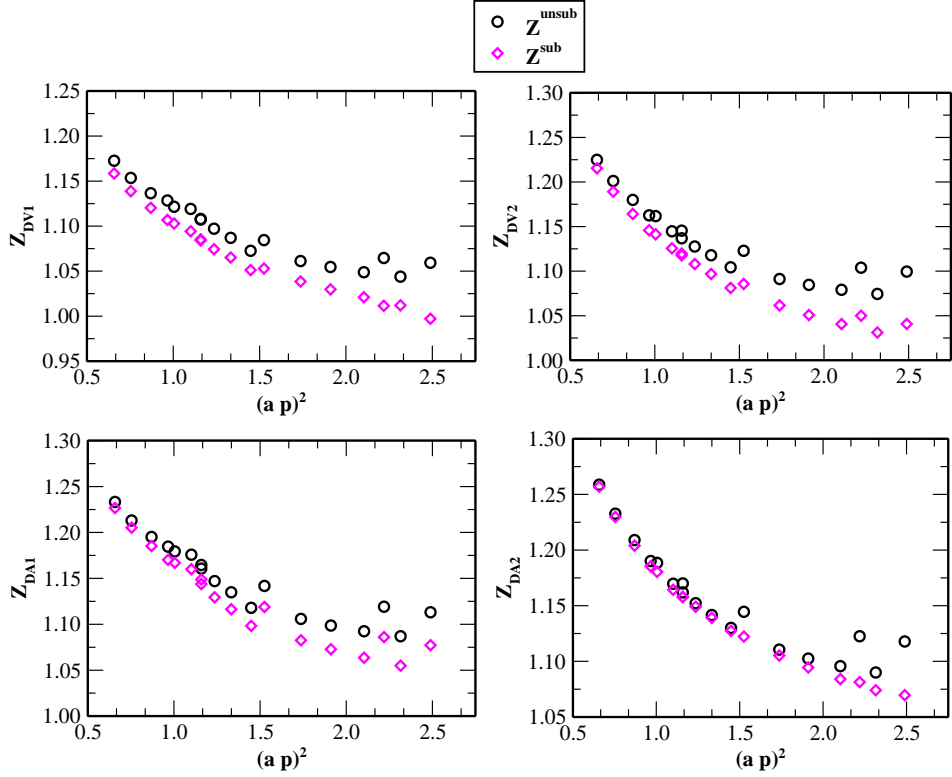


FIG. 9: Renormalization scale dependence for the Z-factors at $\beta = 4.20$ and $m_\pi = 0.476$ GeV

(n_t, n_x, n_y, n_z)	Z_{DV1}	Z_{DV2}	Z_{DA1}	Z_{DA2}
(4,2,2,2)	1.1585(4)	1.215(1)	1.2266(5)	1.257(1)
(5,2,2,2)	1.1387(4)	1.189(1)	1.2052(5)	1.230(1)
(6,2,2,2)	1.1203(3)	1.1642(9)	1.1853(4)	1.2040(9)
(3,3,3,2)	1.1069(2)	1.1459(9)	1.1702(3)	1.1855(9)
(7,2,2,2)	1.1028(2)	1.1413(8)	1.1668(3)	1.1804(8)
(2,3,3,3)	1.0943(2)	1.1257(8)	1.1599(3)	1.1643(8)
(8,2,2,2)	1.0853(1)	1.1197(4)	1.1488(2)	1.1579(4)
(3,3,3,3)	1.0841(1)	1.1177(8)	1.1438(3)	1.1577(8)
(4,3,3,3)	1.0743(2)	1.1079(7)	1.1293(2)	1.1491(7)
(5,3,3,3)	1.0651(2)	1.0968(6)	1.1163(2)	1.1390(6)
(6,3,3,3)	1.0511(2)	1.0812(5)	1.0983(3)	1.1274(5)
(10,2,2,2)	1.0528(1)	1.0856(3)	1.1189(1)	1.1223(3)

TABLE V: Renormalization constants at $\beta = 4.20, \mu_0 = 0.0065$ for lattice size: $32^3 \times 64$.

lattice	Z_{DV1}	Z_{DV2}	Z_{DA1}	Z_{DA2}
$24^3 \times 48$	1.0700(2)	1.0923(2)	1.1190(2)	1.1117(2)
$32^3 \times 64$	1.07123(6)	1.0928(2)	1.12037(7)	1.1122(2)

TABLE VI: Renormalization constants at $\beta = 4.05, \mu_0 = 0.008$ using method 2 and two lattice sizes: $32^3 \times 64$ for (4,4,4,4) and $24^3 \times 48$ for the rest of the momenta.

with

$$R_O(\mu, \mu_0) = \left(\frac{\bar{g}^2(\mu^2)}{\bar{g}^2(\mu_0^2)} \right)^{\frac{\gamma_0^O}{2\beta_0}} \left(\frac{1 + \frac{\beta_1}{\beta_0} \frac{\bar{g}^2(\mu^2)}{16\pi^2}}{1 + \frac{\beta_1}{\beta_0} \frac{\bar{g}^2(\mu_0^2)}{16\pi^2}} \right)^{\frac{1}{2} \left(\frac{\gamma_1^O}{\beta_1} - \frac{\gamma_0^O}{\beta_0} \right)} \quad (61)$$

To 2 loops, the running coupling, β -function and anomalous dimension γ are as follows:

$$\frac{\bar{g}^2(\mu^2)}{16\pi^2} = \frac{1}{\beta_0 \ln(\mu^2/\Lambda^2)} - \frac{\beta_1 \ln \ln(\mu^2/\Lambda^2)}{\beta_0^3 \ln^2(\mu^2/\Lambda^2)} + \dots \quad (62)$$

$$\beta_0 = 11 - \frac{2}{3}N_F, \beta_1 = 102 - \frac{38}{3}N_F \quad (63)$$

$$\gamma^O(g) = \gamma_0^O \frac{g^2}{16\pi^2} + \gamma_1^O \left(\frac{g^2}{16\pi^2} \right)^2 + \dots \quad (64)$$

The expressions for the anomalous dimension of the fermion field and the twist-2 vector/axial operators are given in Ref. [22],

$$\begin{aligned} \gamma_{\psi}^{\text{RI}'}(g) = & 2\lambda C_F \frac{g^2}{16\pi^2} + 2 \left[(9\lambda^3 + 45\lambda^2 + 223\lambda + 225) C_A \right. \\ & \left. - 54C_F - (80\lambda + 72) T_F N_F \right] \frac{C_F}{36} \left(\frac{g^2}{16\pi^2} \right)^2 \end{aligned} \quad (65)$$

$$\begin{aligned} \gamma_{\bar{\psi}\gamma\{\mu D\nu\}\psi}^{\text{RI}'}(g) = & 2\frac{8}{3} C_F \frac{g^2}{16\pi^2} + \frac{2}{54} C_F \left[(27\lambda^2 + 81\lambda + 1434) C_A \right. \\ & \left. - 224C_F - 504 T_F N_F \right] \left(\frac{g^2}{16\pi^2} \right)^2, \end{aligned} \quad (66)$$

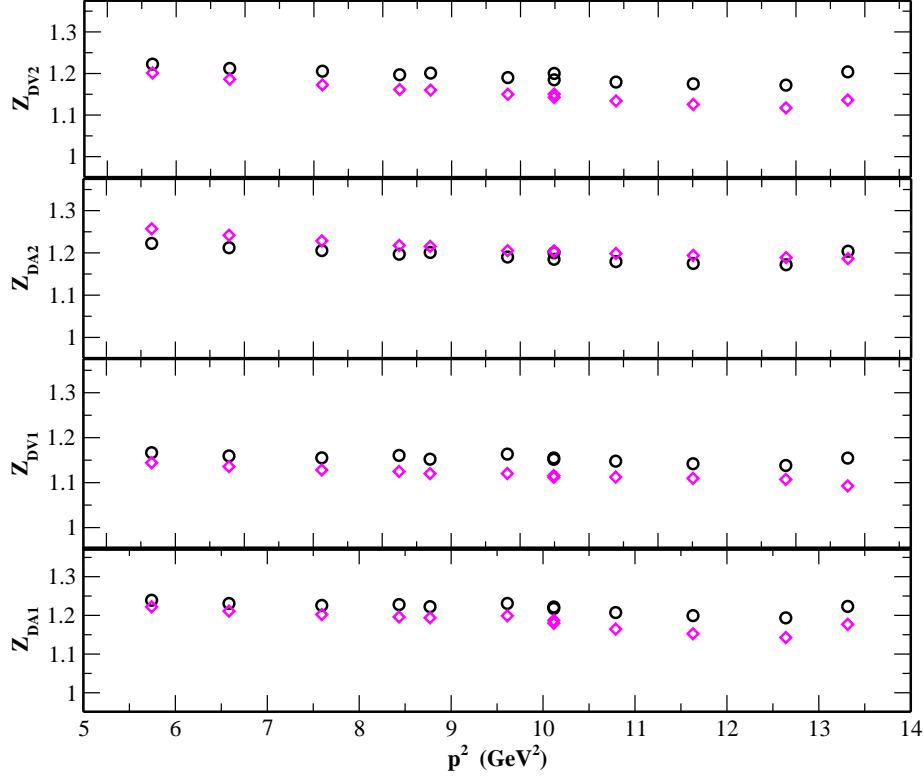


FIG. 10: Renormalization factors in the RI'-MOM scheme at renormalization scale $1/a$, for $\beta = 3.9$, $\mu_0 = 0.0085$. The black circles correspond to the unsubtracted results, while the magenta diamonds to the results with perturbatively subtracted one loop $O(a^2)$ artifacts.

where $T_F = 1/2$, $C_A = N_c$. Using Eqs. (60) - (66) we obtain the Z-factors at $\mu = 1/a$ for $\beta = 3.9$, 4.05, and 4.20, which are plotted in Figs. 10 - 12.

C. Conversion to $\overline{\text{MS}}$

The passage to the continuum $\overline{\text{MS}}$ -scheme is accomplished through use of a conversion factor which is computed up to 3 loops in perturbation theory. By definition, this conversion factor is the same for the vector and axial twist-2 renormalization constant, but will differ for the cases Z_{DV1} (Z_{DA1}) and Z_{DV2} (Z_{DA2}), that is

$$C_{\text{DV1}} \equiv C_{\text{DA1}} = \frac{Z_{\text{DV}}^{\overline{\text{MS}}}}{Z_{\text{DV1}}^{\text{RI}'}} \quad (67)$$

$$C_{\text{DV2}} \equiv C_{\text{DA2}} = \frac{Z_{\text{DV}}^{\overline{\text{MS}}}}{Z_{\text{DV2}}^{\text{RI}'}}. \quad (68)$$

This requirement for different conversion factors results from the fact that the Z-factors in the continuum $\overline{\text{MS}}$ -scheme do not depend on the external indices, μ, ν (see Eq. (2.5) of Ref. [22]), while the results in the RI'-MOM scheme do depend on μ and ν . Of course the conversion factors take a different value for each renormalization scale; actually, the direction of the momentum is required to be known (Eqs. (85) - (86)).

The 3-loop expressions for the conversion factors from our RI'-MOM scheme (Eq. (55)) to the $\overline{\text{MS}}$ do not appear directly in the literature, but can be extracted using results from Ref. [22]. In the latter publication the reader can find the conversion factor from an alternative definition of RI'-MOM (which we denote by RI) to the usual $\overline{\text{MS}}$, $C_{\overline{\psi}\gamma^\mu D^\nu\psi}$. This alternative definition reads

$$\lim_{\epsilon \rightarrow 0} \left[Z_\psi^{\text{RI}} Z_{\overline{\psi}\gamma^\mu D^\nu\psi}^{\text{RI}} \Sigma_{\overline{\psi}\gamma^\mu D^\nu\psi}^{(1)}(p) \right] \Big|_{p^2 = \mu^2} = 1, \quad (69)$$

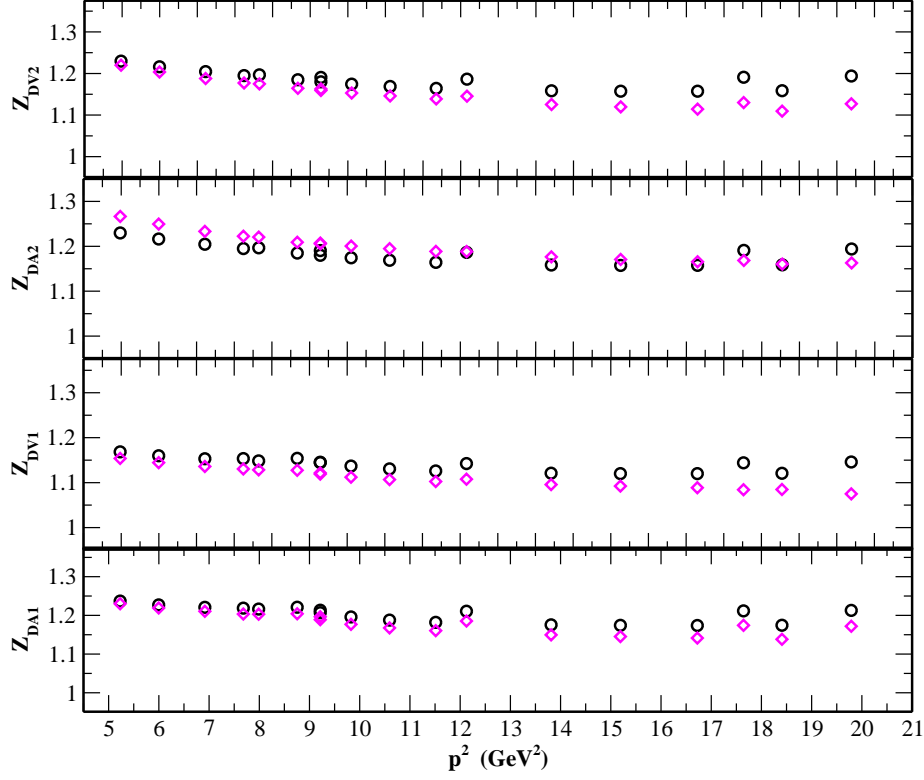


FIG. 11: Same as Fig 10, but for $\beta = 4.05$ and $\mu_0 = 0.008$.

where $\Sigma^{(1)}$ can be extracted from the bare amputated Green's function as follows

$$\begin{aligned}
 G_{\bar{\psi}\gamma\{\mu D\nu\}\psi}^{\mu\nu}(p) &= \langle \psi(p) [\bar{\psi}\gamma^{\{\mu} D^{\nu\}}\psi](0) \bar{\psi}(-p) \rangle \\
 &= \Sigma_{\bar{\psi}\gamma\{\mu D\nu\}\psi}^{(1)}(p) \left(\gamma^\mu p^\nu + \gamma^\nu p^\mu - \frac{2}{d} \not{p} \eta^{\mu\nu} \right) \\
 &\quad + \Sigma_{\bar{\psi}\gamma\{\mu D\nu\}\psi}^{(2)}(p) \frac{1}{p^2} \left(p^\mu p^\nu \not{p} - \frac{p^2}{d} \not{p} \eta^{\mu\nu} \right).
 \end{aligned} \tag{70}$$

The author of Ref. [22] provides the 3-loop expression for the renormalized $\Sigma^{(2)}$ in the scheme of Eq. (69) (note that by definition the renormalized $\Sigma^{(1)}$ equals 1 at $p^2 = \mu^2$). These elements can be used to reconstruct the renormalized Green's function

$$\begin{aligned}
 G_{\bar{\psi}\gamma\{\mu D\nu\}\psi}^{\mu\nu,R}(p) \Big|_{p^2=\mu^2} &= \left[1 \cdot \left(\gamma^\mu p^\nu + \gamma^\nu p^\mu - \frac{2}{d} \not{p} \eta^{\mu\nu} \right) \right. \\
 &\quad \left. + \Sigma_{\bar{\psi}\gamma\{\mu D\nu\}\psi}^{(2)} \text{RI}' \text{ finite}(p) \frac{1}{p^2} \left(p^\mu p^\nu \not{p} - \frac{p^2}{d} \not{p} \eta^{\mu\nu} \right) \right]_{p^2=\mu^2},
 \end{aligned} \tag{71}$$

in which we apply our RI'-MOM condition in order to obtain

$$\frac{Z_{\bar{\psi}\gamma\{\mu D\nu\}\psi}^{\text{RI}}}{Z_{\text{DV1}}^{\text{RI}'}} , \quad \frac{Z_{\bar{\psi}\gamma\{\mu D\nu\}\psi}^{\text{RI}}}{Z_{\text{DV2}}^{\text{RI}'}} \tag{72}$$

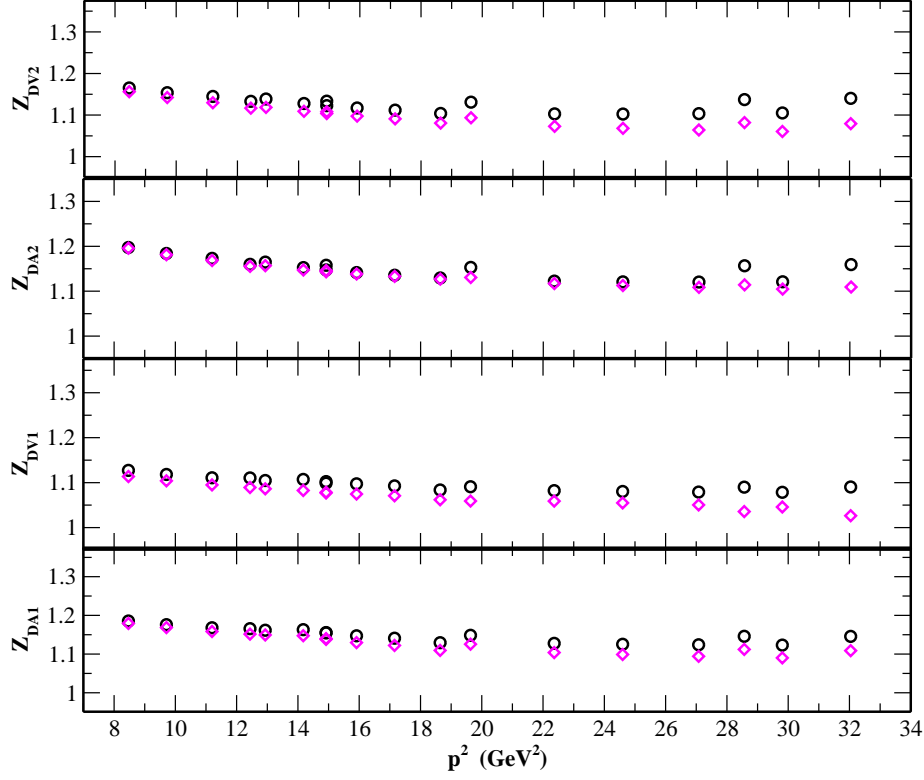


FIG. 12: Same as Fig 10, but for $\beta = 4.20$ and $\mu_0 = 0.0065$.

Once we have these two elements we extract the conversion factor of Eqs. (67) - (68) up to 3 loops,

$$C_{DV1}(\mu) = \frac{Z_{\psi\gamma\{\mu D^\nu\}\psi}^{\text{RI}}}{Z_{DV1}^{\text{RI}'}} \cdot \left(C_{\psi\gamma\mu D^\nu\psi}\right)^{-1} = \frac{Z_{\psi\gamma\{\mu D^\nu\}\psi}^{\text{RI}}}{Z_{DV1}^{\text{RI}'}} \cdot \frac{Z_{DV}^{\overline{\text{MS}}}}{Z_{\psi\gamma\{\mu D^\nu\}\psi}^{\text{RI}}} \quad (73)$$

$$C_{DV2}(\mu) = \frac{Z_{\psi\gamma\{\mu D^\nu\}\psi}^{\text{RI}}}{Z_{DV2}^{\text{RI}'}} \cdot \left(C_{\psi\gamma\mu D^\nu\psi}\right)^{-1} = \frac{Z_{\psi\gamma\{\mu D^\nu\}\psi}^{\text{RI}}}{Z_{DV2}^{\text{RI}'}} \cdot \frac{Z_{DV}^{\overline{\text{MS}}}}{Z_{\psi\gamma\{\mu D^\nu\}\psi}^{\text{RI}}} \quad (74)$$

The conversion to the $\overline{\text{MS}}$ is then given by

$$Z_{DV1}^{\overline{\text{MS}}}(\mu) = C_{DV1}(\mu) \cdot Z_{DV1}^{\text{RI}'}(\mu) \quad (75)$$

$$Z_{DA1}^{\overline{\text{MS}}}(\mu) = C_{DV1}(\mu) \cdot Z_{DA1}^{\text{RI}'}(\mu) \quad (76)$$

and

$$Z_{DV2}^{\overline{\text{MS}}}(\mu) = C_{DV2}(\mu) \cdot Z_{DV2}^{\text{RI}'}(\mu) \quad (77)$$

$$Z_{DA2}^{\overline{\text{MS}}}(\mu) = C_{DV2}(\mu) \cdot Z_{DA2}^{\text{RI}'}(\mu), \quad (78)$$

which correspond to the Z-factors at the same renormalization scale in the RI'. One wants to obtain the renormalization constants at the scale of 2 GeV, and to do this we use the 2-loop formula in Eq. (61)-(62) to evolve the scale from μ to 2 GeV. In these formulas we need to insert the anomalous dimension in the $\overline{\text{MS}}$ -scheme which read [22]

$$\gamma_{\psi\gamma\{\mu D^\nu\}\psi}^{\overline{\text{MS}}}(\alpha) = 2 \frac{8}{3} C_F \alpha + 2 \frac{8 C_F}{27} [47 C_A - 14 C_F - 16 T_F N_F] \alpha^2 \quad (79)$$

where $\alpha = g^2/(16\pi^2)$. The additional factor of 2 that we included, comes from the different definition of the anomalous dimension that leads to Ref. [23]. To summarize, the Z-factors in the continuum $\overline{\text{MS}}$ -scheme at $\mu = 2$ GeV are given

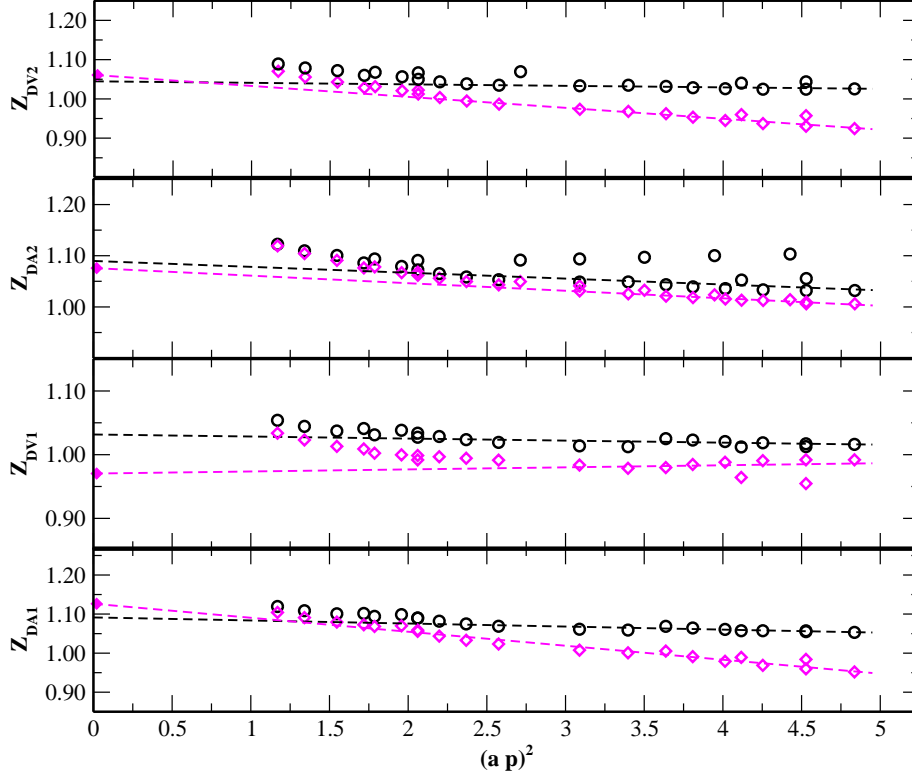


FIG. 13: Renormalization factors at $\beta = 3.9$, $\mu_0 = 0.0085$ in the $\overline{\text{MS}}$ -scheme at renormalization scale 2 GeV. Black circles correspond to the unsubtracted results, while magenta diamonds correspond to the results with perturbatively subtracted 1-loop $O(a^2)$ artifacts. The lines show extrapolations to $a^2 p^2 = 0$ using the subtracted results within the range $a^2 p^2 = 3 - 5$.

by

$$Z_{\text{DV1}}^{\overline{\text{MS}}}(2\text{GeV}) = R_{\text{DV}}(2\text{GeV}, \mu) \cdot C_{\text{DV1}}(\mu) \cdot Z_{\text{DV1}}^{\text{RI}'}(\mu) \quad (80)$$

$$Z_{\text{DV2}}^{\overline{\text{MS}}}(2\text{GeV}) = R_{\text{DV}}(2\text{GeV}, \mu) \cdot C_{\text{DV2}}(\mu) \cdot Z_{\text{DV2}}^{\text{RI}'}(\mu) \quad (81)$$

$$Z_{\text{DA1}}^{\overline{\text{MS}}}(2\text{GeV}) = R_{\text{DV}}(2\text{GeV}, \mu) \cdot C_{\text{DV1}}(\mu) \cdot Z_{\text{DA1}}^{\text{RI}'}(\mu) \quad (82)$$

$$Z_{\text{DA2}}^{\overline{\text{MS}}}(2\text{GeV}) = R_{\text{DV}}(2\text{GeV}, \mu) \cdot C_{\text{DV2}}(\mu) \cdot Z_{\text{DA2}}^{\text{RI}'}(\mu) \quad (83)$$

$$(84)$$

For the $SU(N_c = 3)$ colour group ($C_A = 3$, $C_F = 4/3$, $T_F = 1/2$), Landau gauge ($\lambda = 0$), and general quark flavours, we have the following conversion factors

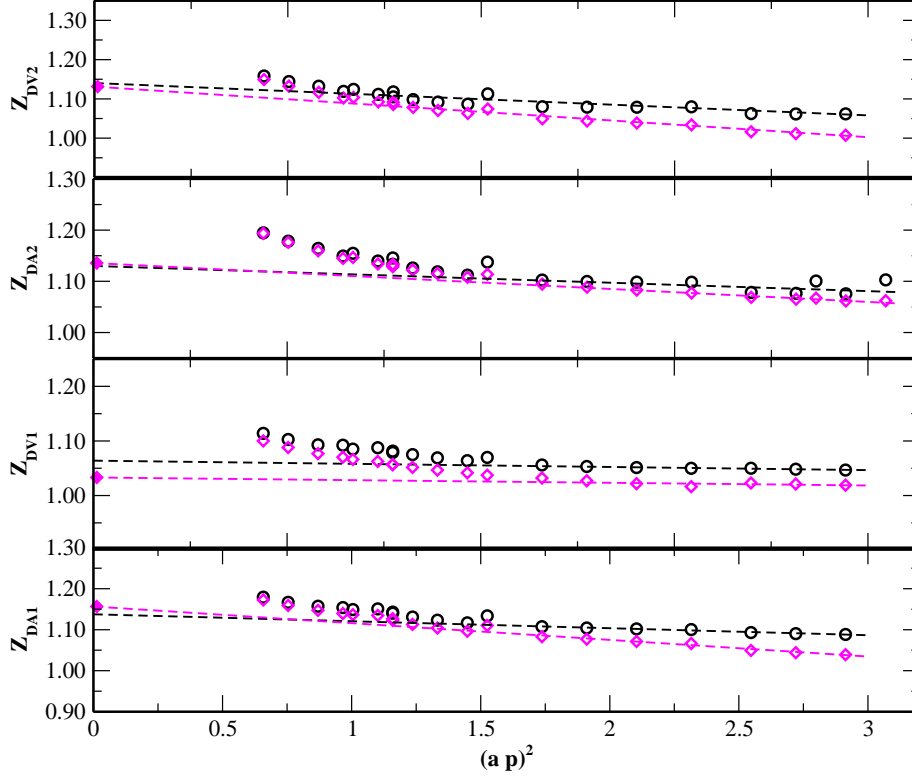


FIG. 14: Renormalization factors at $\beta = 4.05$, $\mu_0 = 0.008$ in the $\overline{\text{MS}}$ -scheme at renormalization scale 2 GeV. The black circles correspond to the unsubtracted results, while the magenta diamonds to the results with perturbatively subtracted one loop $O(a^2)$ artifacts. The lines show extrapolations to $a^2 p^2 = 0$ using the subtracted results within the range $a^2 p^2 = 1.9 - 3$.

$$\begin{aligned}
C_{DV1} \equiv \frac{Z_{DV}^{\overline{\text{MS}}}}{Z_{DV1}^{\text{RI}'}} &= 1 + \alpha \left[-\frac{136}{27} + \frac{64}{9} \frac{\mu_\mu^2 - \frac{\mu_\mu^4}{\mu^2}}{\mu^2 + 8\mu_\mu^2} \right] \\
&+ \alpha^2 \left[-\frac{128096}{729} + N_F \left(\frac{3208}{243} - \frac{320}{9} \frac{\mu_\mu^2 - \frac{\mu_\mu^4}{\mu^2}}{\mu^2 + 8\mu_\mu^2} \right) + \frac{248}{9} \zeta(3) + \frac{\mu_\mu^2 - \frac{\mu_\mu^4}{\mu^2}}{\mu^2 + 8\mu_\mu^2} \left(\frac{17792}{27} + \frac{320}{9} \zeta(3) \right) \right] \\
&+ \alpha^3 \left[-\frac{627867571}{78732} - \frac{64\pi^4}{729} + \frac{5588641}{2187} \zeta(3) + N_F^2 \left(-\frac{149552}{6561} + \frac{77440}{729} \frac{\mu_\mu^2 - \frac{\mu_\mu^4}{\mu^2}}{\mu^2 + 8\mu_\mu^2} - \frac{256}{243} \zeta(3) \right) \right. \\
&\quad \left. + N_F \left(\frac{19947676}{19683} + \frac{64\pi^4}{243} - \frac{1600}{27} \zeta(3) + \frac{\mu_\mu^2 - \frac{\mu_\mu^4}{\mu^2}}{\mu^2 + 8\mu_\mu^2} \left(-\frac{121024}{27} + \frac{9856}{81} \zeta(3) \right) \right) \right. \\
&\quad \left. - \frac{19420}{27} \zeta(5) + \frac{\mu_\mu^2 - \frac{\mu_\mu^4}{\mu^2}}{\mu^2 + 8\mu_\mu^2} \left(\frac{270701210}{6561} - \frac{2993992}{243} \zeta(3) + \frac{349600}{81} \zeta(5) \right) \right] + \mathcal{O}(\alpha^4) \quad (85)
\end{aligned}$$

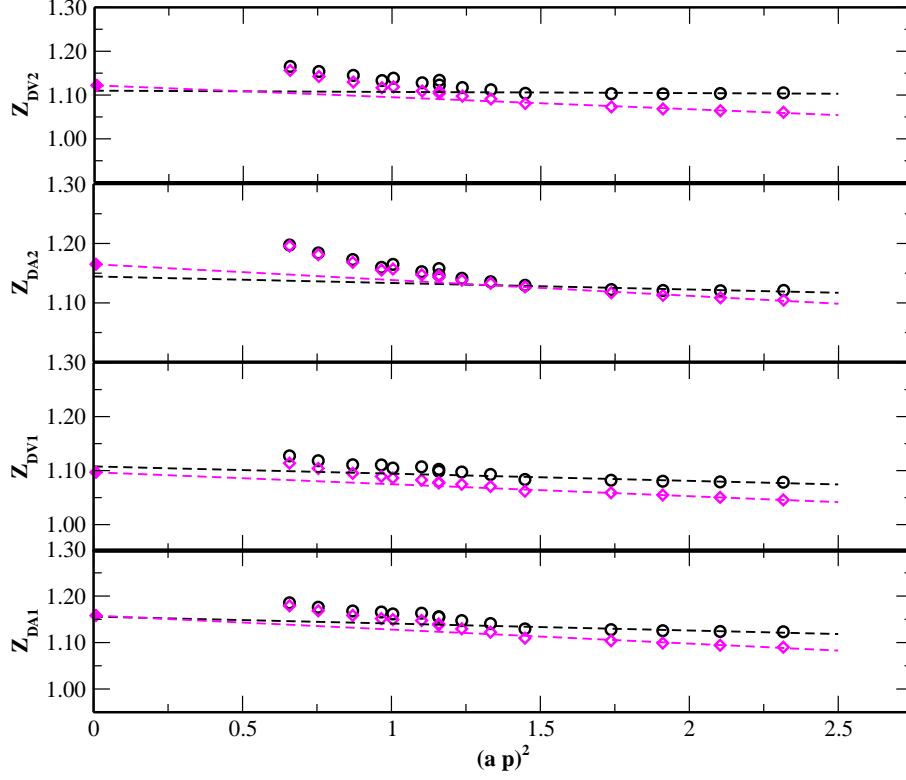


FIG. 15: Renormalization factors at $\beta = 4.20$, $\mu_0 = 0.0065$ in the $\overline{\text{MS}}$ -scheme at renormalization scale 2 GeV. The black circles correspond to the unsubtracted results, while the magenta diamonds to the results with perturbatively subtracted one loop $O(a^2)$ artifacts. The lines show extrapolations to $a^2 p^2 = 0$ using the subtracted results within the range $a^2 p^2 = 1.2 - 2.5$.

$$\begin{aligned}
C_{\text{DV2}} \equiv \frac{Z_{\text{DV}}^{\overline{\text{MS}}}}{Z_{\text{DV1}}^{\text{RI}'}} &= 1 + \alpha \left[-\frac{124}{27} - \frac{16}{9} \frac{\mu_\mu^2 \mu_\nu^2}{\mu^2(\mu_\mu^2 + \mu_\nu^2)} \right] \\
&+ \alpha^2 \left[-\frac{98072}{729} + N_F \left(\frac{2668}{243} + \frac{80}{9} \frac{\mu_\mu^2 \mu_\nu^2}{\mu^2(\mu_\mu^2 + \mu_\nu^2)} \right) + \frac{268}{9} \zeta(3) + \frac{\mu_\mu^2 \mu_\nu^2}{\mu^2(\mu_\mu^2 + \mu_\nu^2)} \left(-\frac{4448}{27} - \frac{80}{9} \zeta(3) \right) \right] \\
&+ \alpha^3 \left[-\frac{849683327}{157464} - \frac{64 \pi^4}{729} + \frac{7809041}{4374} \zeta(3) + N_F^2 \left(-\frac{105992}{6561} - \frac{19360}{729} \frac{\mu_\mu^2 \mu_\nu^2}{\mu^2(\mu_\mu^2 + \mu_\nu^2)} - \frac{256}{243} \zeta(3) \right) \right. \\
&\quad \left. + N_F \left(\frac{14433520}{19683} + \frac{64 \pi^4}{243} - \frac{4184}{81} \zeta(3) + \frac{\mu_\mu^2 \mu_\nu^2}{\mu^2(\mu_\mu^2 + \mu_\nu^2)} \left(\frac{30256}{27} - \frac{2464}{81} \zeta(3) \right) \right) \right. \\
&\quad \left. - \frac{36410}{81} \zeta(5) + \frac{\mu_\mu^2 \mu_\nu^2}{\mu^2(\mu_\mu^2 + \mu_\nu^2)} \left(-\frac{135350605}{13122} + \frac{748498}{243} \zeta(3) - \frac{87400}{81} \zeta(5) \right) \right] + \mathcal{O}(\alpha^4) \quad (86)
\end{aligned}$$

where $\alpha = g^2/(16\pi^2)$ and $\zeta(n)$ is the Riemann Zeta function.

A “renormalization window” should exist for $\Lambda_{QCD}^2 \ll \mu^2 \ll 1/a^2$ where perturbation theory holds and finite- a artifacts are small, leading to scale-independent results (plateau). In practice such a condition is hard to satisfy: The right inequality is extended to $(2-5)/a^2$ leading to lattice artifacts in our results that are of $\mathcal{O}(a^2 p^2)$. Fortunately our perturbative calculations allow us to subtract the leading perturbative $O(a^2)$ lattice artifacts which alleviates the problem. To remove the remaining $O(a^2 p^2)$ artifacts we extrapolate linearly to $a^2 p^2 = 0$ as demonstrated in Figs. 13 -15. The statistical errors are negligible and therefore an estimate of the systematic errors is important. We note that, in general, the evaluation of systematic errors is difficult. The largest systematic error comes from the choice of the momentum range to use for the extrapolation to $a^2 p^2 = 0$. One way to estimate this systematic error is to vary the momentum range where we perform the fit. Another approach is to fix a range and then eliminate a given

momentum in the fit range and refit. The spread of the results about the mean gives an estimate of the systematic error. In the final results we give as systematic error the largest one from using these two procedures which is the one obtained by modifying the fit range. We choose the same momentum range in physical units for all β -values and we thus extract all renormalization constants using the same physical momentum range, $p^2 \sim 15 - 32 \text{ (GeV)}^2$. This momentum range has been chosen so that we are in a region where an approximate plateau is seen at each β . We also note that the $\mathcal{O}(a^2)$ perturbative terms which we subtract, decrease as β increases, as expected and the values extracted from subtracted and unsubtracted data agree when extrapolated to $a = 0$. The momentum range in lattice units at each β is as follows: $\beta = 3.9 : a^2 p^2 \sim 3 - 5$, $\beta = 4.05 : a^2 p^2 \sim 1.9 - 3$, $\beta = 4.20 : a^2 p^2 \sim 1.2 - 2.5$ and as can be seen in Figs. 13 -15 within these ranges the data fall on a straight line of a small slope. Our final results for the Z -factors in the $\overline{\text{MS}}$ -scheme at 2 GeV are given in Table VII, which have been obtained by extrapolating linearly in $a^2 p^2$, using the fixed momentum range $p^2 \sim 15 - 32 \text{ (GeV)}^2$.

β	Z_{DV1}	Z_{DV2}	Z_{DA1}	Z_{DA2}
3.90	0.970(34)(26)	1.061(23)(29)	1.126(22)(78)	1.076(5)(1)
4.05	1.033(11)(14)	1.131(23)(18)	1.157(9)(7)	1.136(5)
4.20	1.097(4)(6)	1.122(7)(10)	1.158(7)(7)	1.165(5)(10)

TABLE VII: Renormalization constants Z_{DV} and Z_{DA} in the $\overline{\text{MS}}$ scheme. The above values have been obtained by extrapolating linearly in $a^2 p^2$. Statistical errors are shown in the first parenthesis. The error in the second parenthesis is the systematic error due to the extrapolation, namely the difference between results using the fit range $p^2 \sim 15 - 32 \text{ (GeV)}^2$ and the range $p^2 \sim 17 - 24 \text{ (GeV)}^2$. An error smaller than the last digit given for the mean value is not quoted.

VI. CONCLUSIONS

The values of the renormalization factors for the one-derivative twist-2 operators are calculated non-perturbatively. The method of choice is to use a momentum dependent source and extract the renormalization constants for all the relevant operators. This leads to a very accurate evaluation of these renormalization factors using a small ensemble of gauge configurations. The accuracy of the results allows us to check for any light quark mass dependence. For all the renormalization constants studied in this work we do not find any light quark mass dependence within our small statistical errors. Therefore it suffices to calculate them at a given quark mass. We also show that, despite of using lattice spacing smaller than 1 fm, $\mathcal{O}(a^2)$ effects are sizable. We perform a perturbative subtraction of $\mathcal{O}(a^2)$ terms. This leads to a smoother dependence of the renormalization constants on the momentum values at which they are extracted. Residual $\mathcal{O}(a^2 p^2)$ effects are removed by extrapolating to zero. In this way we can accurately determine the renormalization constants in the RI'-MOM scheme. In order to compare with experiment we convert our values to the $\overline{\text{MS}}$ scheme at a scale of 2 GeV. The statistical errors are in general smaller than the systematic. The latter are estimated by changing the window of values of the momentum used to extrapolate to $a^2 p^2 = 0$. Our final values are given in Table VII.

VII. ACKNOWLEDGMENTS

This work was partly supported by funding received from the Cyprus Research Promotion Foundation under contracts EPYAN/0506/08, and TECHNOLOGY/ΘΕΙΠΣ/0308(BE)/17.

-
- [1] S. Durr et al., Science **322**, 1224 (2008).
 - [2] C. Alexandrou et al. (ETM), Phys. Rev. **D80**, 114503 (2009), arXiv:0910.2419.
 - [3] X.-D. Ji, J. Phys. **G24**, 1181 (1998), hep-ph/9807358.
 - [4] P. Hagler et al. (LHPC), Phys. Rev. **D68**, 034505 (2003), hep-lat/0304018.
 - [5] P. Hagler et al. (LHPC), Phys. Rev. **D77**, 094502 (2008), arXiv:0705.4295.
 - [6] S. N. Syritsyn et al. (2009), arXiv:0907.4194.
 - [7] D. Brommel et al. (QCDSF-UKQCD), PoS **LAT2007**, 158 (2007), arXiv:0710.1534.
 - [8] C. Alexandrou et al. (ETMC) (2008), arXiv:0811.0724.
 - [9] T. Yamazaki et al., Phys. Rev. **D79**, 114505 (2009), arXiv:0904.2039.

- [10] C. Alexandrou et al., PoS **LAT2009**, 145 (2009), arXiv:0910.3309.
- [11] C. Alexandrou et al., PoS **LAT2009**, 136 (2009).
- [12] M. Constantinou, H. Panagopoulos, and F. Stylianou, PoS **LAT2009**, 205 (2009).
- [13] C. Alexandrou, M. Constantinou, T. Korzec, H. Panagopoulos, and F. Stylianou, *in preparation*.
- [14] P. Weisz, Nucl. Phys. **B212**, 1 (1983).
- [15] M. Constantinou, V. Lubicz, H. Panagopoulos, and F. Stylianou, JHEP **10**, 064 (2009), arXiv:0907.0381.
- [16] G. P. Lepage and P. B. Mackenzie, Phys. Rev. **D48**, 2250 (1993), hep-lat/9209022.
- [17] P. Dimopoulos et al., PoS **LAT2007**, 241 (2007), arXiv:0710.0975.
- [18] P. O. L. Zhaofeng, V. Morenas, *private communication*.
- [19] M. Gockeler et al., Nucl. Phys. **B544**, 699 (1999), hep-lat/9807044.
- [20] P. de Forcrand, Nucl. Phys. Proc. Suppl. **9**, 516 (1989).
- [21] M. Constantinou et al., JHEP **08**, 068 (2010), 1004.1115.
- [22] J. A. Gracey, Nucl. Phys. **B667**, 242 (2003), hep-ph/0306163.
- [23] E. G. Floratos, D. A. Ross, and C. T. Sachrajda, Nucl. Phys. **B129**, 66 (1977), erratum, *ibid.*, B139, 545-546 (1978).